SRF

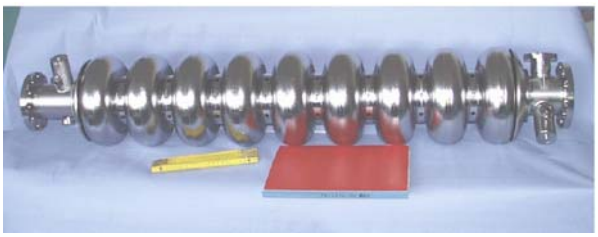

2.2.1.14 MS Final Reports for new components: Cold Flanges

P. Michelato, L. Monaco, N. Panzeri

INFN Milano - LASA, Milano, Italy

Abstract

In this note, we report the critical analysis of the behavior of a TESLA like beamline flange connection, both at room and at cryogenic (LN_2) temperature. Several compression tests on this joint have been performed to measure the sealing mechanical properties and the leak rate behavior at different loads. The development of a dedicated model for FEM analysis is also presented and its results have been compared with the experimental ones. Finally, a simple analytical model that describes the flanges connection behavior including the temperature effects is discussed.

Index

1 Introduction

An analysis of main ancillaries of SRF cavities is going on, to highlight possible criticalities in achieving both better performances and higher reliability for future large accelerator facilities, like ILC (International Linear Collider). Among the main ancillaries of a SRF cavity, defined in our previous report [1], flange connections play a crucial role and an improvement of their reliability is required for the future SRF accelerator structures. A simple numerical example shows the importance of the reliability improvement: about 20000 cavities will be assembled in the ILC and several thousands of cold flanges will be used. Therefore, the reliability of the seal, the reduction of costs of flanges and seals, the decrease of seal assembly and tightening time, the shortening of the junction dimensions and the increase of the machine filling factor are key points. To study this problem, tests have already been done in different laboratories and with different type of joints, both at room and at cryogenic temperature [2], [3], [4], [5].

In this document we present a critical analysis of the TESLA beamline connection flanges at room and at cryogenic temperature, with dedicated experimental measurements and with the development of a model for FEM analysis. Results so far obtained give information on their behavior, on their leak tightening limit, etc. The main result, after the experimental validation of the model, is the possibility to study the seal behavior changing the compression force, the groove and seal geometry, the gasket material, etc.

In the following section, after a short description of the experimental set-up used for compression tests, the measurements done both at room and cryogenic temperature are discussed. Moreover, results of leak tests are presented.

In sections 3 and 4, we present respectively the FEM analysis model and a simple analytical model that describes the flanges connection including the temperature effects.

2 Experimental tests

Some experimental tests have been performed on different gaskets in order to understand their behavior at room and cryogenic temperature. In particular, the following procedure has been adopted:

- compression tests at room temperature by means of a material testing machine capable to compress up to 200 kN. During some of these tests a leak detector has also been used;
- compression tests at room temperature using bolts as a means to apply the load. Also in some of these tests a leak detector has been used;
- sealing tests at cryogenic temperature (77 K, LN_2).

In the following subsections we present the methodology adopted and the results obtained.

2.1 An introduction to the cold sealing problem in SC accelerator

A superconducting accelerator is characterized by extremely good vacuum condition (UHV) in the accelerator structure, due to the low temperature of the surfaces that act as a cryogenic pump for all gases except He and H_2. Many of the demountable connections (flanges), that are along the beamline, stay inside the cryostats immersed in the insulation vacuum. The eventually leaks on these flanges act as a connection between the UHV and the "dirty" environment of the insulation vacuum chamber. This may produce the condensation of various gases and vapors on the niobium surface. Moreover if the insulation vacuum is in equilibrium with helium leaks (from He tanks), helium will enter the beamline where can not be cryopumped and has to be pumped by ion getter pumps. If the flanges act as a separation between liquid helium bath (HeI or HeII) and the beamline vacuum, the reliability of the tightness of the flanges is a must. These connections have to guarantee a reliable sealing both at room and cryogenic temperature, also after thermal cycles that may occur in the life of the accelerator.
Referring to TESLA cavities, junctions are realized by demountable connections, composed by two different flanges (male and female) and an aluminum alloy gasket.
As reported in the literature [6], [7] the "quality" of a demountable seal depends on many parameters as: the flanges geometry, the materials and finishing (roughness), the mechanical properties and the geometry of the material used for the seal, the way how the force is applied (distribution, elasticity of the compression system) etc. In a simplified model, the plasticity of the seal will be correlated with the capability of materials to close imperfections and scratches while the elastic behavior of the seal will compensate small movements produced for instance by temperature change.
Moreover, it is well known that some general parameters can be used to qualify or to compare the sealing quality: one of these is the specific force on the seal (N/m) and the pressure exerted on the sealing surface. Both depend on the geometry while the second is correlated with the capability of the seal to reduce the conductance of the leak path [7].

2.2 Geometry and material of specimens

As reported in the introduction, in our study we have taken as reference the TESLA beam line connection. Its geometry is reported in Figure 1, Figure 2 and Figure 3 with the indication of the parts material.

For our tests we machined two flanges as similar as possible to the original ones (see Figure 4), and one of them (the blank one) was realized in two different materials: stainless steel (AISI 304) and NbTi 45/55. Stainless steel flanges were used for room temperature tests while, for the sealing tests at LN_2 temperature, a NbTi and a SS blank flange have been used in order to correctly evaluate the temperature effects.

As far as concern the gasket, two materials are used: Al5754 (AlMgSi0.5) and Al6060 (AlMg3). Each gasket was numbered and, at the end of mechanical test, chemically analyzed in order to evaluate the Mg contents and check its correspondence to EN codes. The list of tested gaskets is reported in Table 1. As a last the bolts used were A4 -70 (AISI 316) and the nuts in CuNiSil.

Al 6060 family		Al 5754 family	
Gasket name	Mg %	Gasket name	Mg %
G #02*	0.438	G #13	2.674
G #03	0.44	G #14	2.962
G #04⊗	0.446	G #15	2.954
G #06	0.439	G #16	2.983
G #07◊	0.441	G #18	2.73
G #10	0.438	G #20	2.71
G #11	0.439	G #24	2.96
G #12	0.437	G #25	2.968
G #19	0.44	G #38	2.956
G #27	0.441	G #39	2.978
G #29	0.437	G #40	2.973
G #31	0.433		
G #32	0.44		
G #34	0.445		

Table 1: gaskets used for tests.

* used for compression test by means of mechanical machine

⊗ used for compression test by means of manual tightening at cryogenic temperature

◊ used for compression test by means of manual tightening

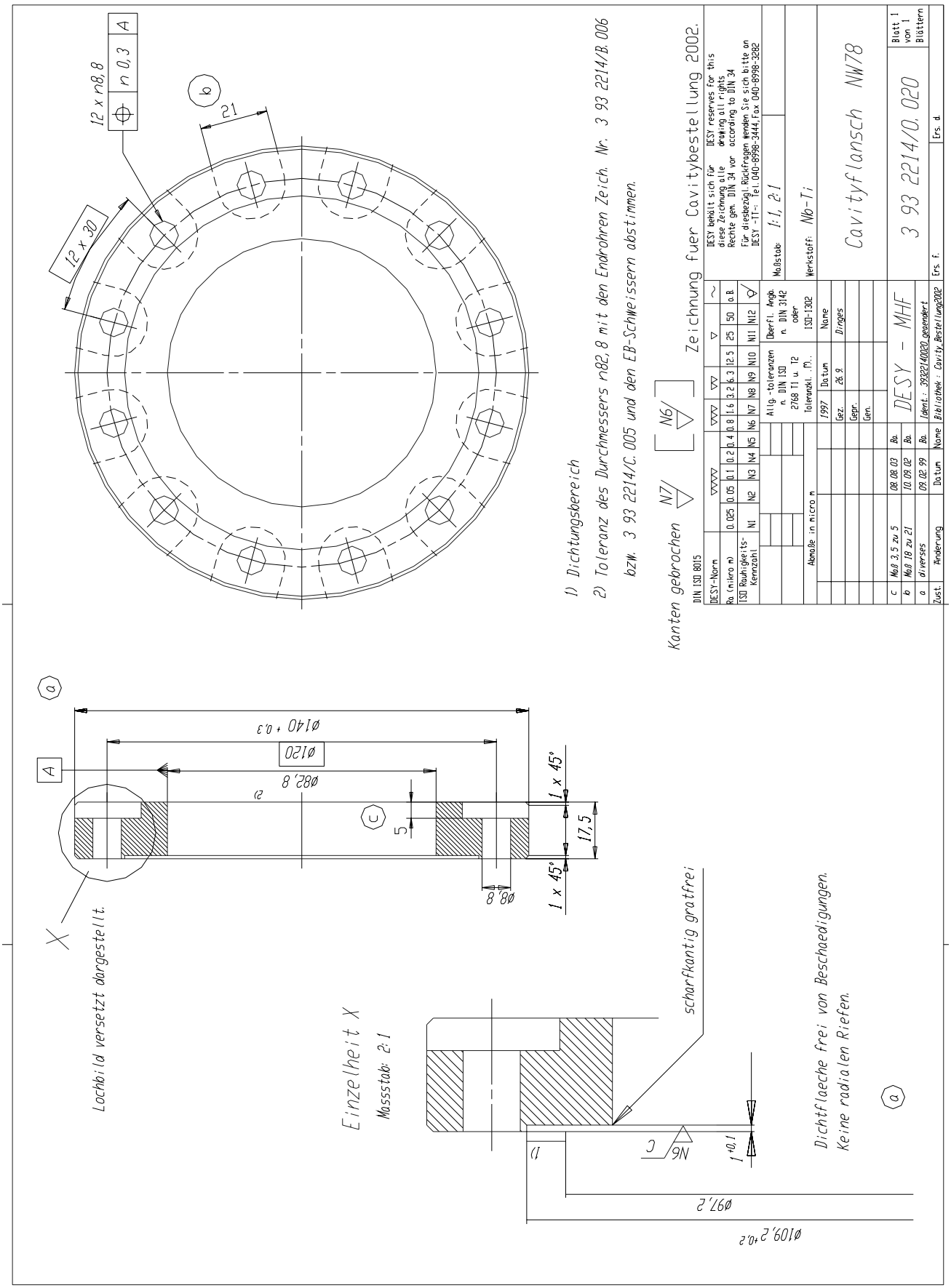

Figure 1: male flange geometry.

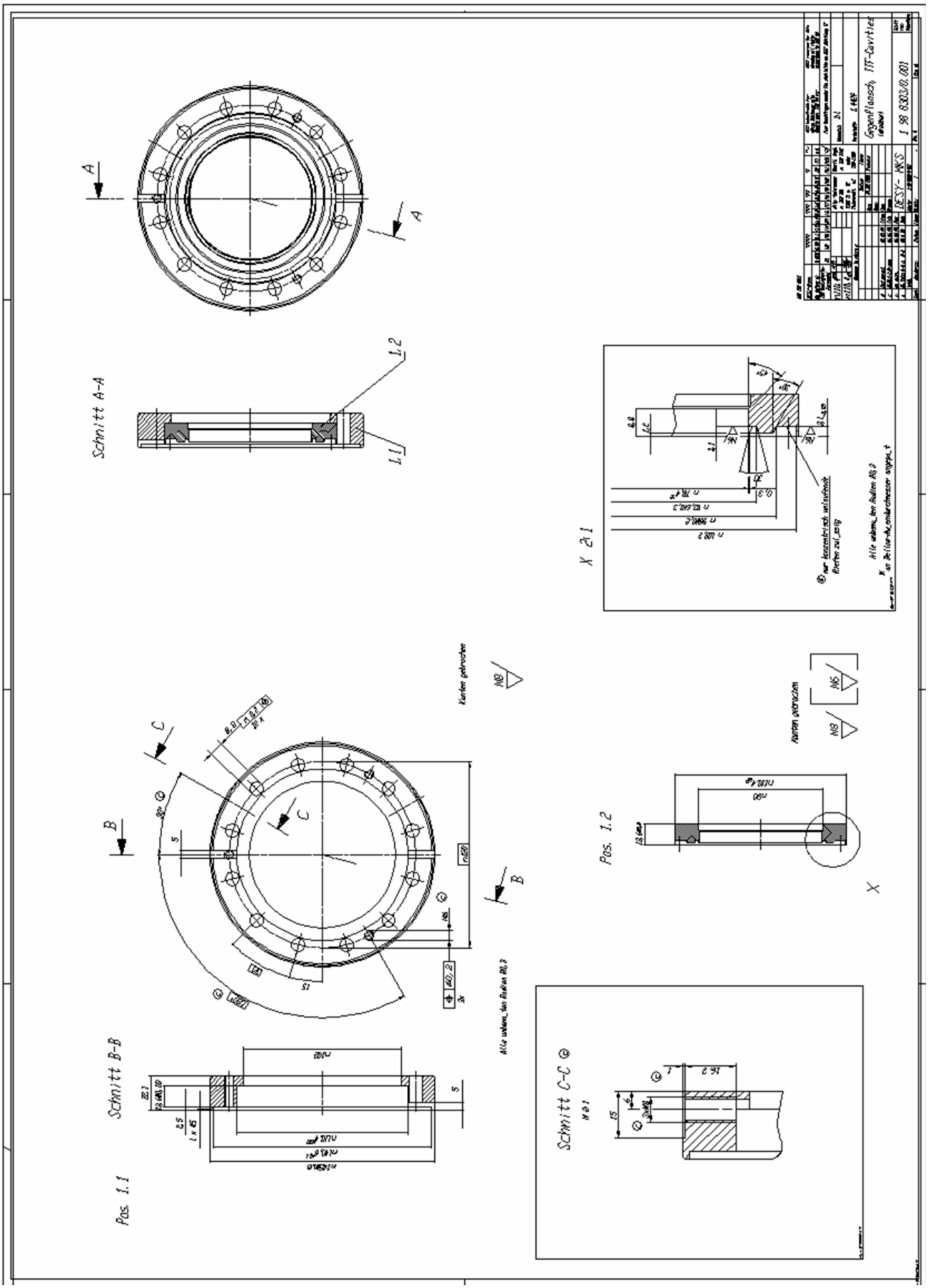

Figure 2: female flange geometry.

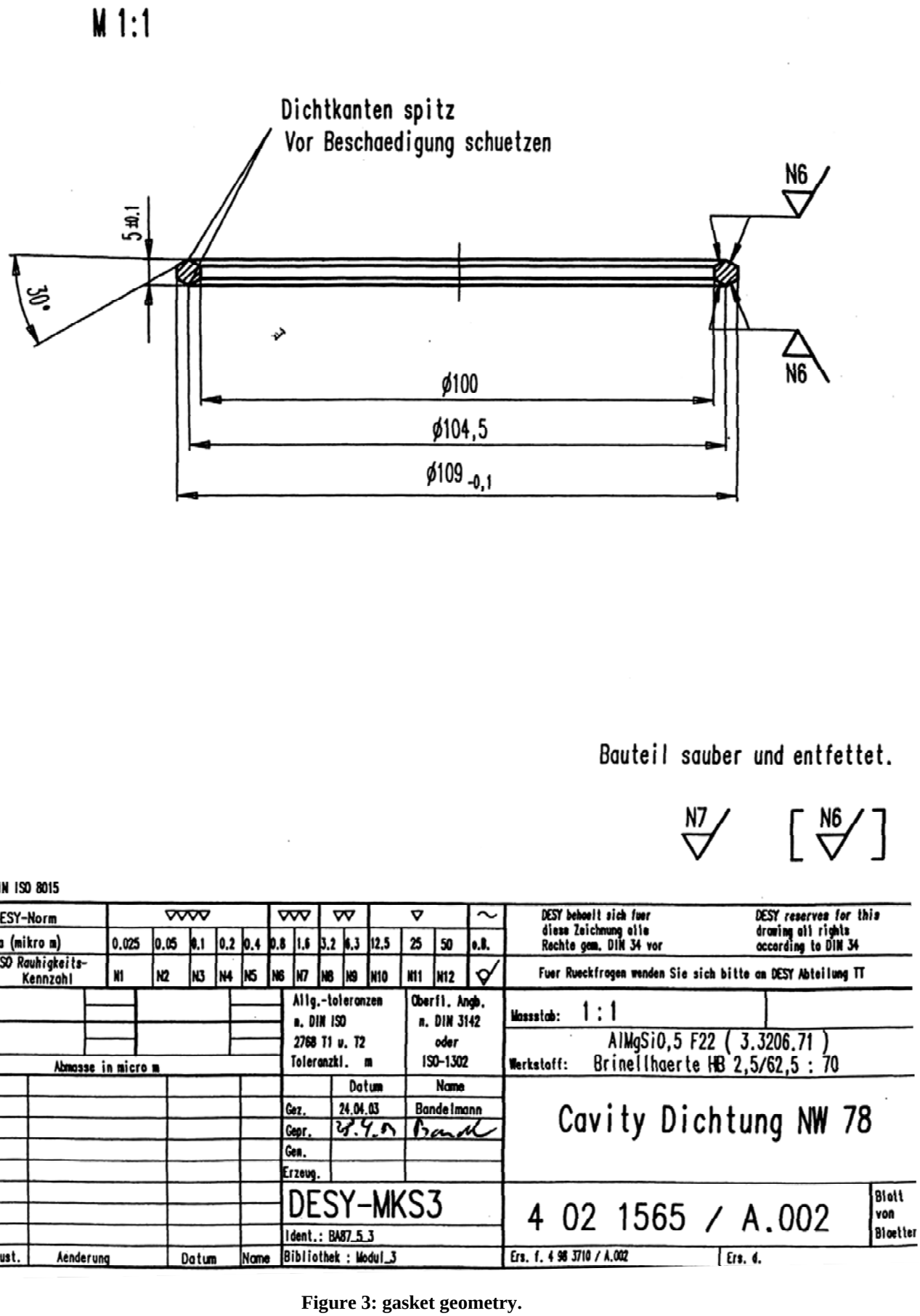

Figure 3: gasket geometry.

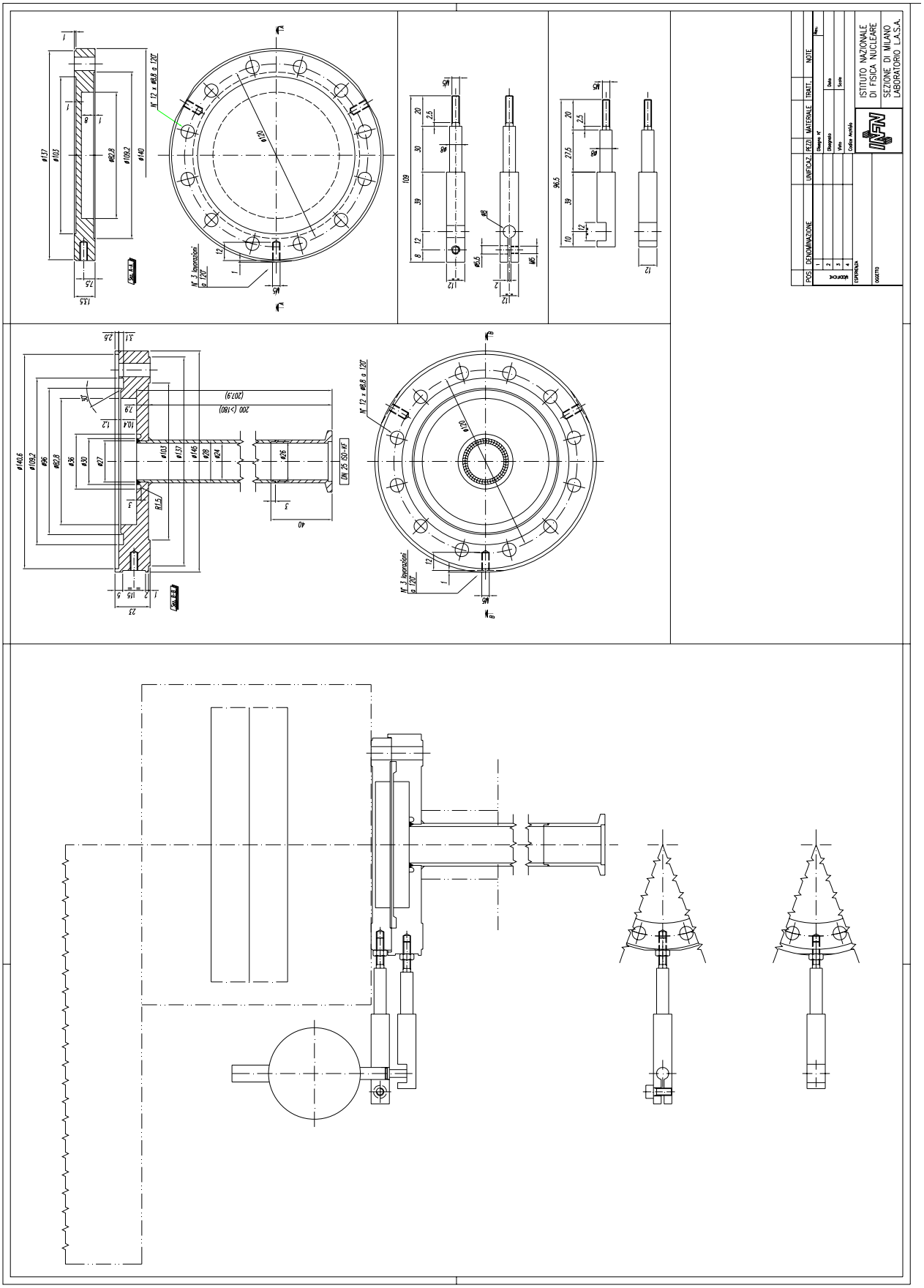

Figure 4: flanges used in our experimental tests.

2.3 Compression tests using a material testing machine

In order to understand the sealing behavior and to obtain data for the validation of the numerical model presented in section 3, we performed some compression tests of gaskets typically used in the TTF beamline flange connections. Two type of diamond shape gaskets have been used for the beamline connection, whose mainly difference is the material composition (Al5754 and Al6060), while the geometry is the same. Tests have been done on both family gaskets to critically analyze their behavior in sealing.

2.3.1 Test set-up

A material testing machine (INSTRON, model 6027), capable to apply a maximum load of 200 kN with a precision of 0.5%, has been used for these compression tests (see Figure 5). In particular the specimens (assembly of flanges and gasket) were put between the load cell and the movable frame cross member of the machine (see Figure 6). Because of specimens high stiffness (half of the stiffness of the testing machine), a spherical joint has been used in order to avoid any damage to the load cell. The weight of this joint is of 50 N.

Figure 5: the Instron machine used for the compression tests.

Figure 6: a particular of the flanges in the test machine and the electronic gauges applied to them.

The displacement transducer of the test machine can not be directly used because it would record not only the displacement of the flanges but also the deformations of the machine frame, therefore three electronic gauges (Digimatic indicator, Mitutoyo 543-250B-70, resolution 0.001mm, accuracy 0.003mm) were applied to the flanges side and used as displacement reading device. Unfortunately, for reasons that will be explained in the following, also these measurements revealed itself not correct and a manual micrometer (Mitutoyo 293-801, 0.001mm of resolution) was used to measure the relative displacement of the two flanges. Furthermore, during the seal compression, leak tests have been also performed in order to check the seal efficiency, using a calibrated leak detector (UL200, Leybold, sensitivity $1 \cdot 10^{-10}$ mbar l/s). A representation of the experimental apparatus is shown in Figure 7.

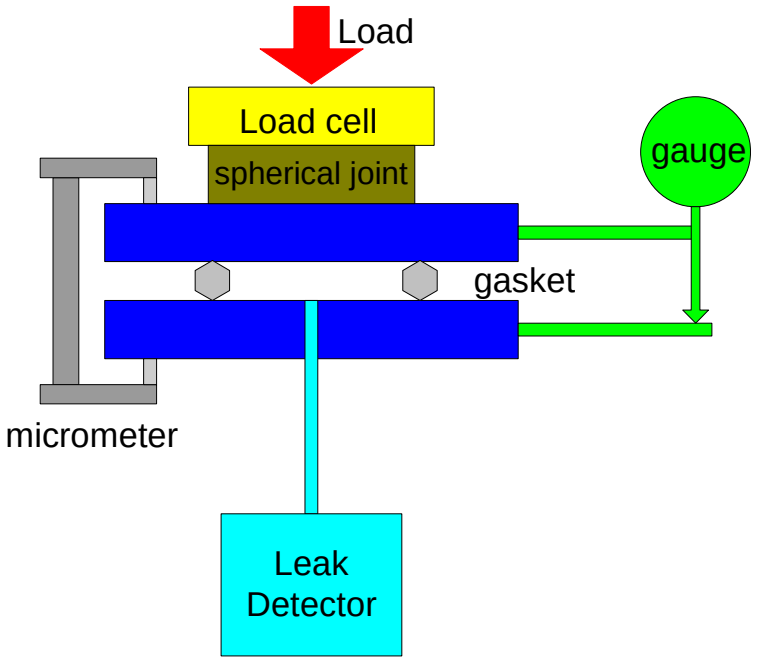

Figure 7: sketch of the experimental apparatus used for compression test.

The tests have been performed in displacement control at different velocities, from 6 μm/min to 24 μm/min but it has been found that this parameter does not influence the results (at least in this range). During the tests the machine frame cross member displacement, the three gauges and the leak detector output have been constantly read and their values recorded every 3 seconds.
The normal loading history consists of a first compression up to 195 kN and an unloading to 10 kN followed by a second compression up to 195 kN and a final unloading. Only in few cases the maximum compression load applied was less than this limit. When the manual measurement with the micrometer was needed, the tests were stopped for the time necessary for the reading.
Only for Al6060 gaskets (G #10 and G #11) the procedure was different because we wanted to obtain the flattening data as a function of the compression forces as explained in section 2.3.3.

2.3.2 Compression force – squashing results

A typical curve is reported in Figure 8: it is important to note that the displacement recorded by the Instron machine is larger than the one allowable by the flange geometry (0.9 mm maximum). This “error” is due to the deformation of the Instron machine that is not negligible.

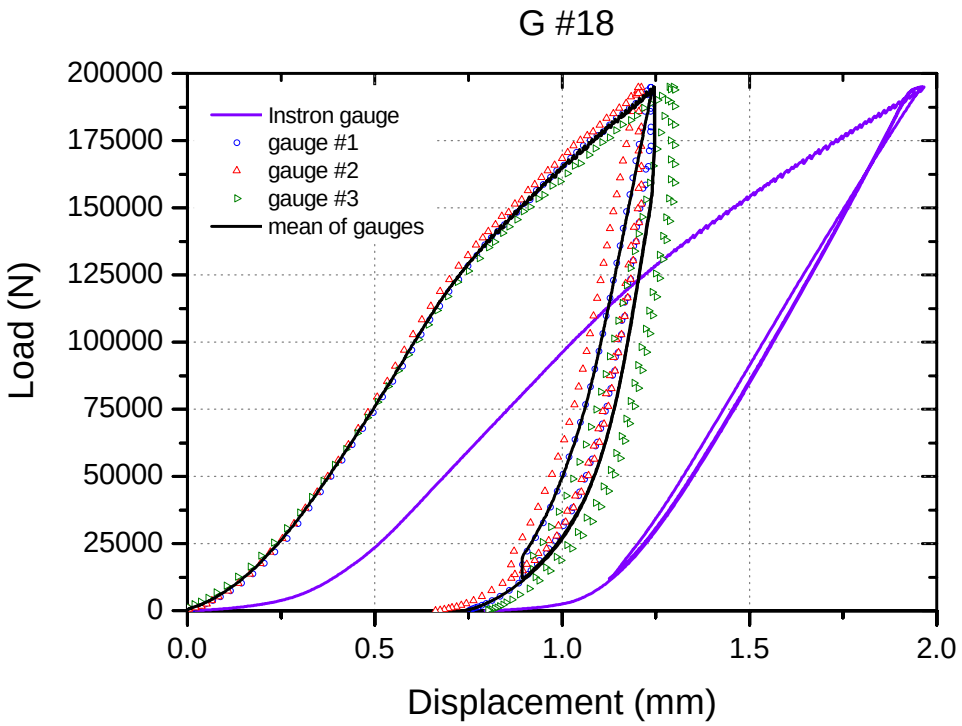

Figure 8: force - displacement curve of gasket #18. Measurements obtained by Instron and by the three gages (with the mean value) are also reported.

A more correct graph should be obtained when gauges mean displacements are used. Unfortunately we discovered that also these measures were affected by an error due to the bending of the flanges. Therefore we have calibrated our system realizing dedicated tests in which the displacements were measured not only by electronic and Instron gauges, but also with a manual micrometer. The method followed to obtain the error curve is described in section 2.3.2.1. This error curve has then be subtracted to all the displacements recorded by the Instron machine gauge in order to obtain the real force – displacement relations of the gaskets.

2.3.2.1 Procedure followed to obtain the error curve

The total measurement obtained by Instron gauge and by the external ones is affected by the deformations of the flanges and of the machine frame. This error can be considered depending only on the force and the measured displacement can be expressed as the sum of different terms expanded in the following relation:

$$\delta_m = \delta_g(F;t) + \delta_e(F)$$

where δ_m is the measured displacement by the machine gauge, δ_g is the gasket squashing that depends on the force applied and on the material type and finally δ_e represents the error due to the deformation of machine frame. A reasonable assumption is that the error depends linearly from the force except for low compression forces where the behavior can not be linear because of the assessment of mechanical slack.

Therefore, in order to evaluate the error of the measured displacement by the Instron gauge, the real squashing of the gasket has been measured at different load level using a micrometer. The procedure has been applied to three compression tests performed up to 170 kN on different gaskets (G#15 and G#25 Al5754, G#34 Al6060). The values obtained by the micrometer and the Instron gauge have then been compared (see Figure 9) and an error curve has been obtained (see Figure 10). It is evident how the error curve does not depend from the

material type of the gasket and the hypothesis of its linearity is satisfied for compression force higher than 20 kN.

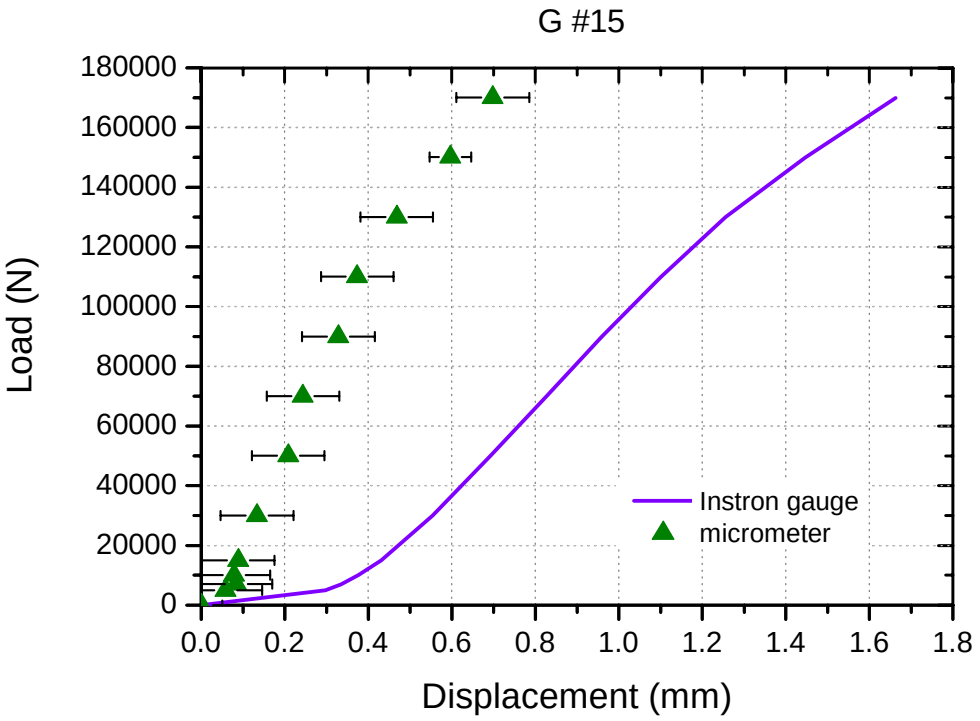

Figure 9: displacement measured by the manual micrometer and the Instron gauge (G #15 – Al5754).

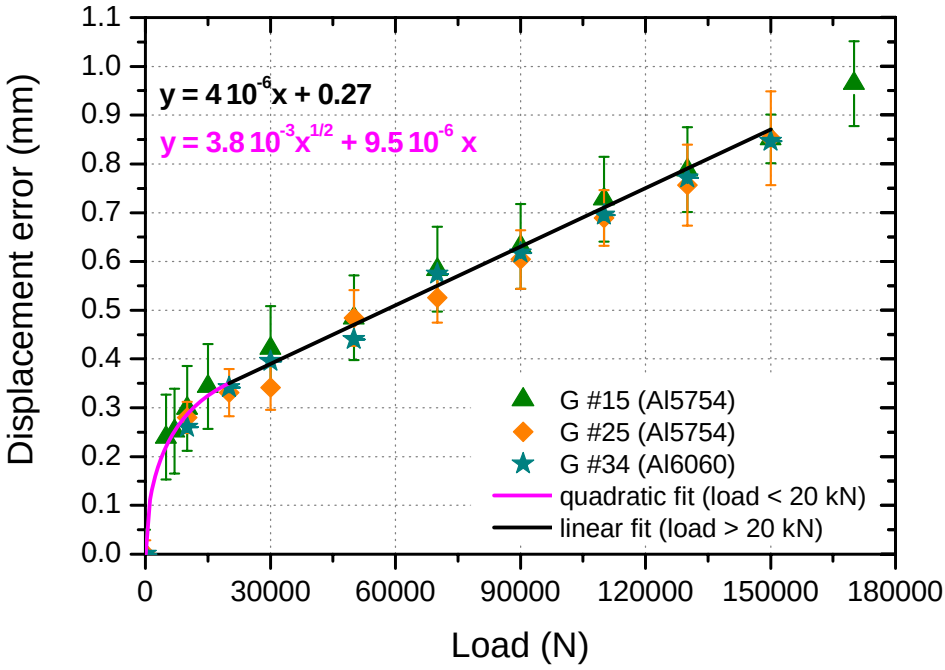

Figure 10: error curve of the displacement recorded with the Instron machine as a function of the applied force.

Using the two fits, linear for loads higher than 20 kN and quadratic for loads lower than 20 KN, it is possible to correct the displacement recorded by the Instron machine, as shown in Figure 11, where the wrong curve and the corrected one are reported. For sake of control, the

data recorded by the micrometer for gasket G #15 are also reported and their good agreement with the corrected curve of gasket G #18 confirms the correctness of the adopted procedure.

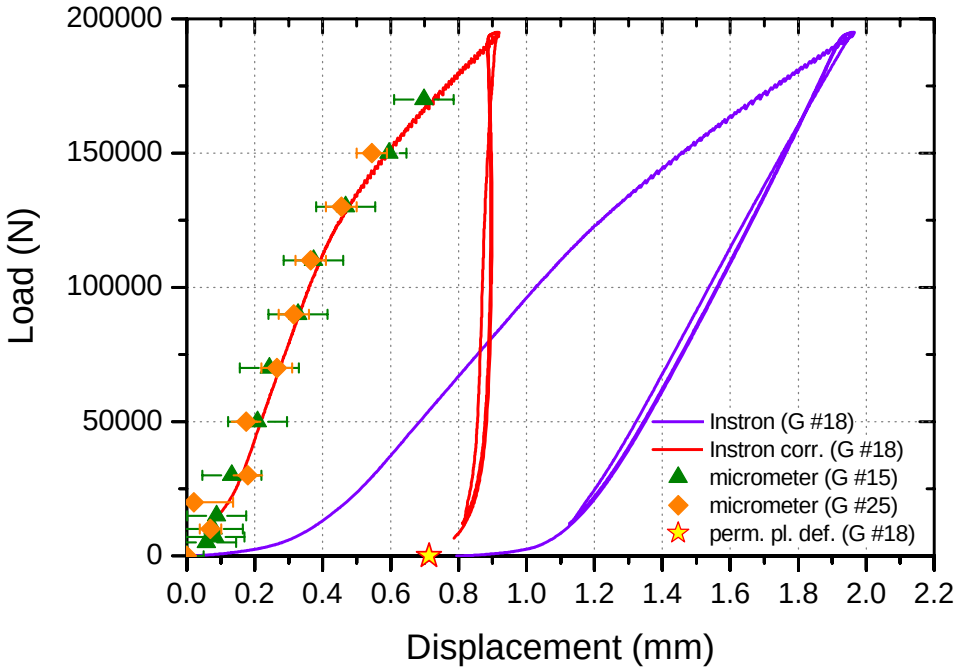

Figure 11: comparison between the load displacement of gasket G #18 measured by the Instron gage before and after the correction. The displacement of gasket G #15 and G #25 are also reported.

2.3.2.2 All compression corrected results

In this section a summary of all compression measurements (maximum load applied 190 kN) realized on several gaskets of the two families is reported (Figure 12). Plots have been corrected using the fit described in the previous section. All measurements have been obtained loading and unloading gaskets, following the procedure described in section 2.3.

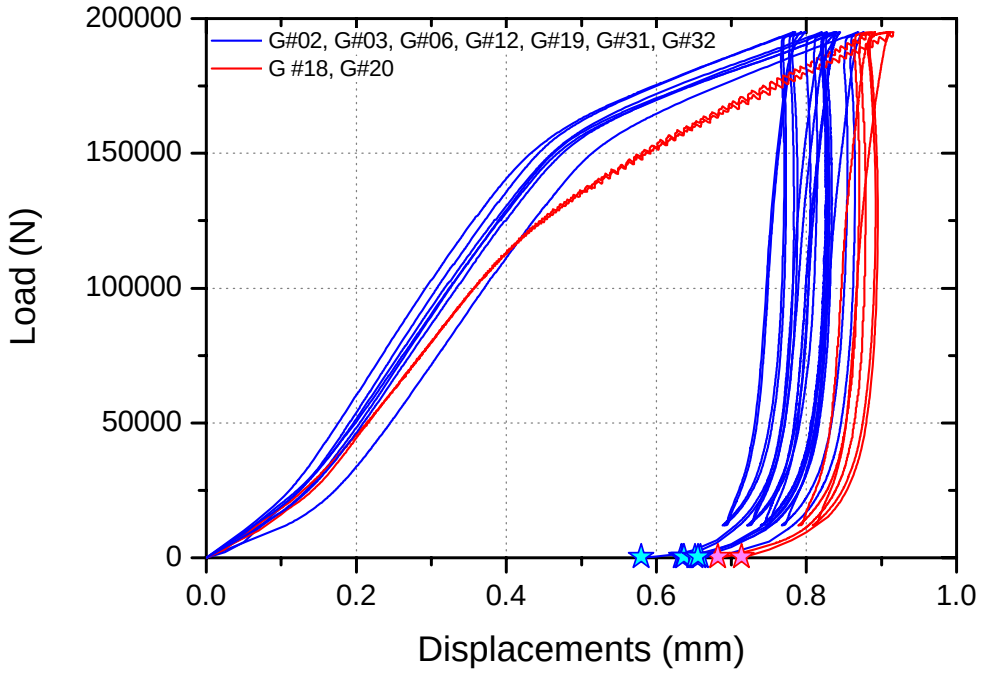

Figure 12: summary of all Instron compression test. Results of two gasket families are plotted together for comparison.

The two gasket families behave differently under compression. Referring to gasket G #20 and G #18 (Al5754), their behavior at the increasing of the load is different if compared with the other gaskets (all of Al6060), not only for the total displacement measured at 190 kN but also for the shape of the curves during the first compression. Displacements of the Al5754 grow smoothly with the load and, on the contrary, Al6060 gaskets show a steeper increase (up to 150 kN) followed by a flattened behavior toward 190 kN. At the end of the first compression, the total displacement at 190 kN is 0.877 ± 0.016 mm for the Al5754 gaskets and 0.822 ± 0.003 mm for the Al6060 gaskets.
Referring to the first unloading curve, we can obtain the total elastic recovery capability of the gaskets analyzed, measuring the permanent squashing at zero load and comparing it to the maximum displacement. For the two families we obtain: 0.178 ± 0.006 mm for the Al5754 and 0.186 ± 0.024 mm for the Al6060.
Two typical curves, obtained for gasket G #18 (Al5754) and gasket G #03 (Al6060), are shown in Figure 13. A picture of these gaskets after compression cycles are reported in Figure 14, where the surface aspects, after compression test, are strongly different.

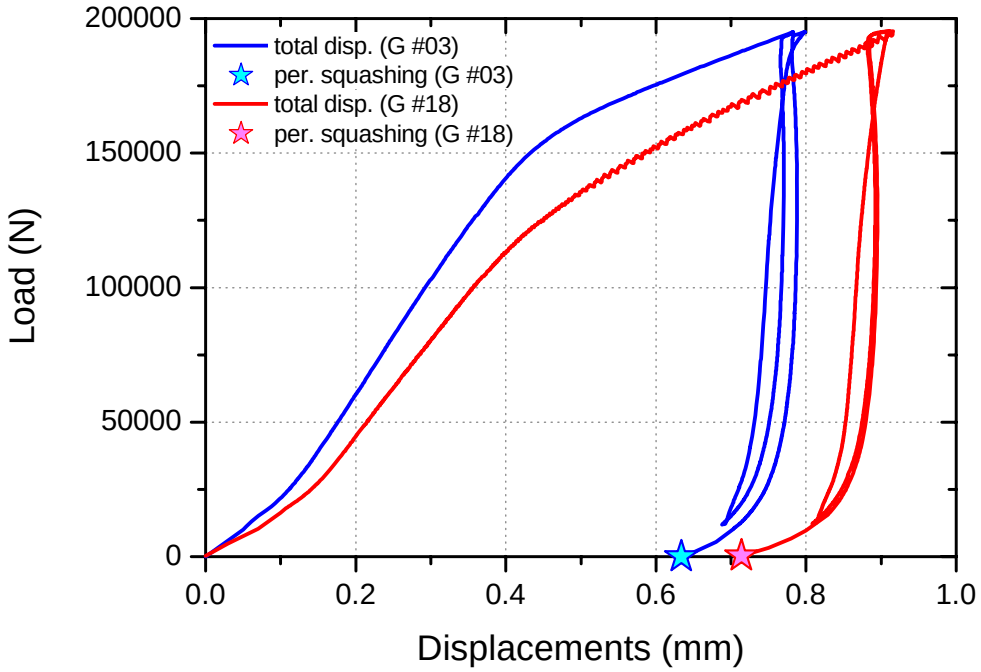

Figure 13: Instron compression test of gasket G #18 and gasket G #03. In the figure also the permanent squashing of the two gaskets is reported.

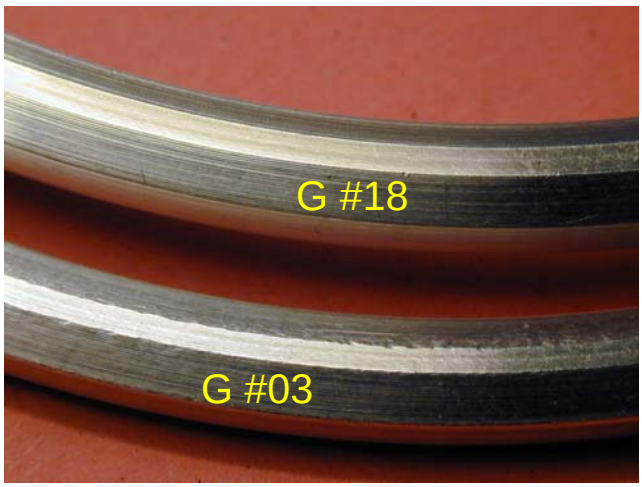

Figure 14: photos of gasket #18 and gasket #03 after the compression cycles.

After compression tests, all gaskets have been measured to determine their permanent shape deformations due to the compression cycles. We measured their permanent squashing and their flattening, defined as the amplitude of the gasket contact region (discussed in the following section). In Figure 15 permanent squashing of all gaskets is reported. From this plot it is evident the difference between the two families: the Al6060 plastic deformation is lower than the one measured for Al5754 family at the same load level.

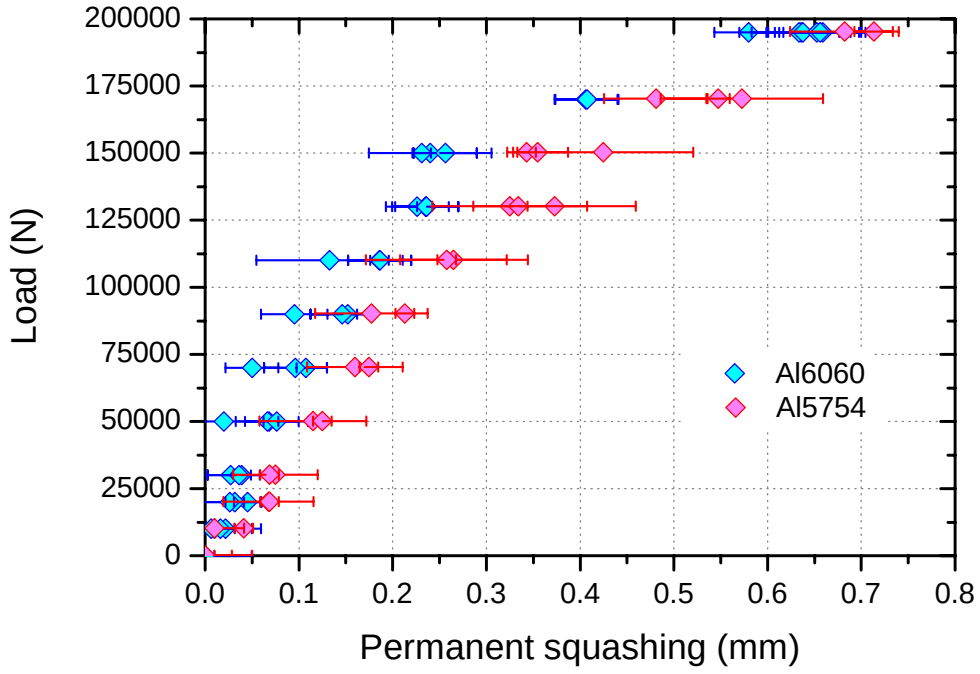

Figure 15: summary of permanent squashing of all measured gaskets.

2.3.3 Flattening results

As pointed out in section 2.1 the sealing depends both on the pressure applied to the gasket and on the width of the contact surface (see Figure 16). An higher pressure will reduce the effective amplitude of the conductance by reducing the effective area. Moreover, the increase of the contact surface will increase the length of leak path that will decrease the conductance [7].

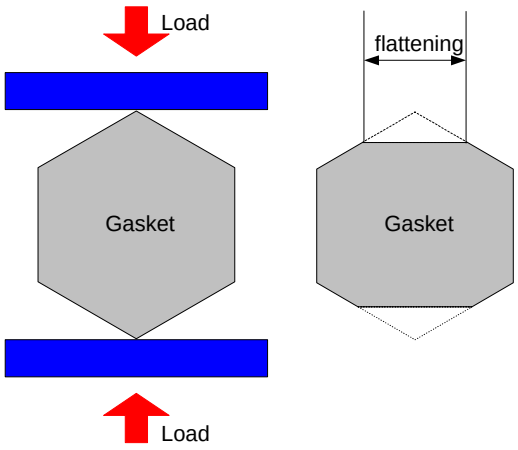

Figure 16: gasket flattening.

Flattening have been measured for all tested gaskets and their values are reported in Figure 17.

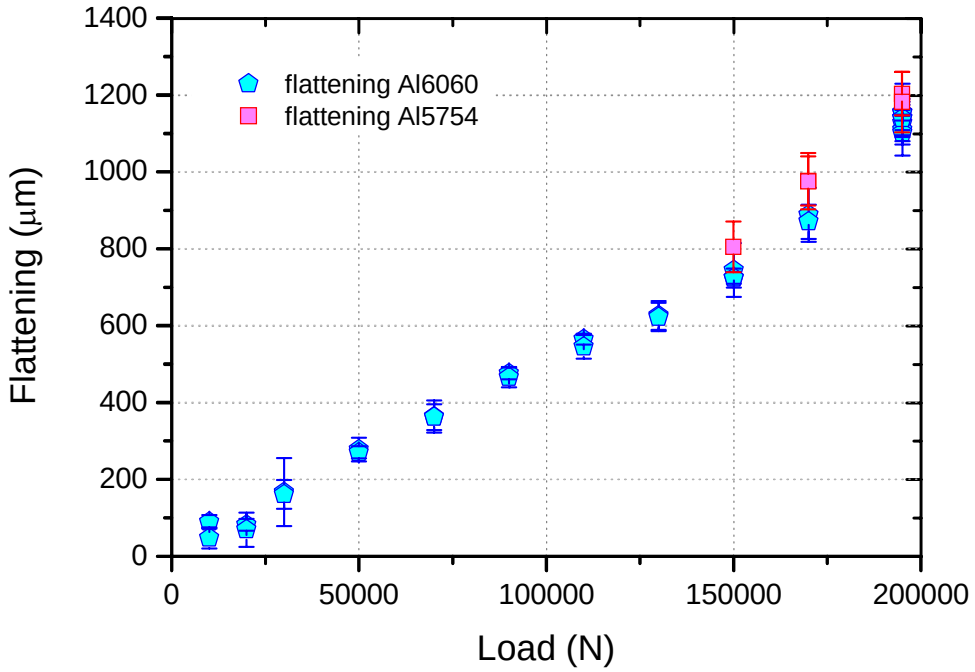

Figure 17: flattening of several gaskets after the compression tests.

In particular, for gasket G #10 and G #11 the final load was applied in different loading-unloading steps such as to be able to measure the gasket flattening at different load levels (see Figure 18). On the same plot we have also reported the value of the pressure on the contact region area as a function of the compression force. This figure shows the typical data for an Al6060 alloy gasket: the gasket flattening increases linearly with the load and hence the pressure stays almost constant and equal to the strength of the material.

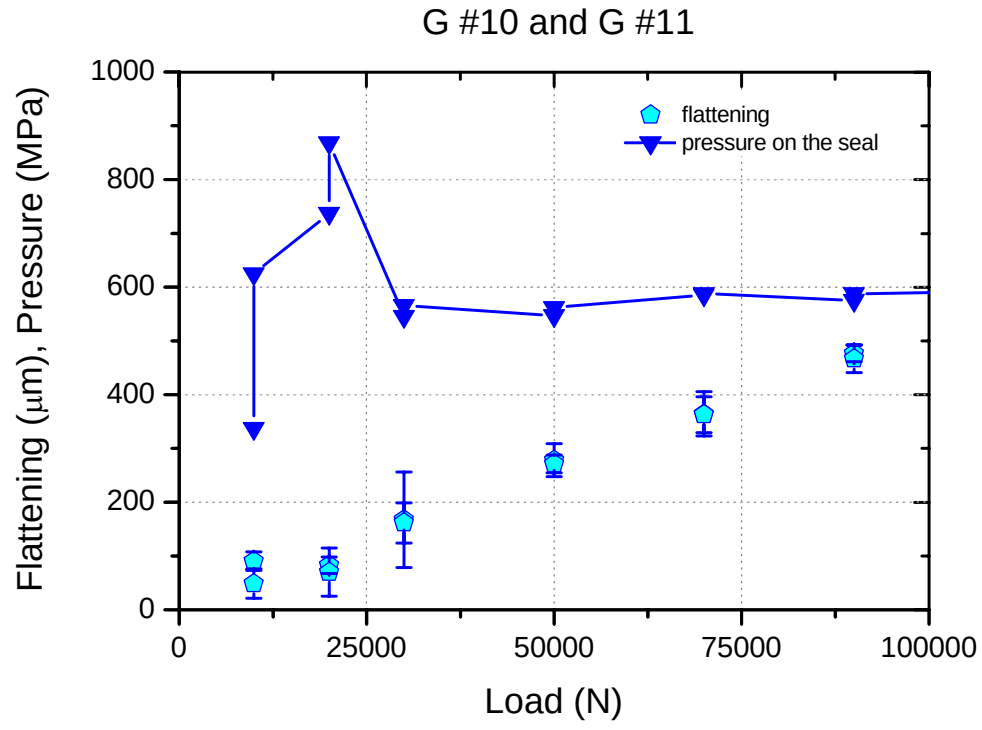

Figure 18: flattening and pressure vs. load applied of gaskets G #10 and G #11.

2.3.4 Leak rate results

During compression measurements, leak tests have been performed in order to study the generation of the seal and the behavior of the leak rate vs. the load applied to the flanges. The leak test starts at the early beginning of the seal generation, and, in these conditions, the leak rate is quite high: this produces in some measurements a strong He background signal, whose subtraction reflects some uncertainty in the leak test. As an example the leak behavior during a compression test is shown (gasket G #03 - Al6060) in Figure 19.

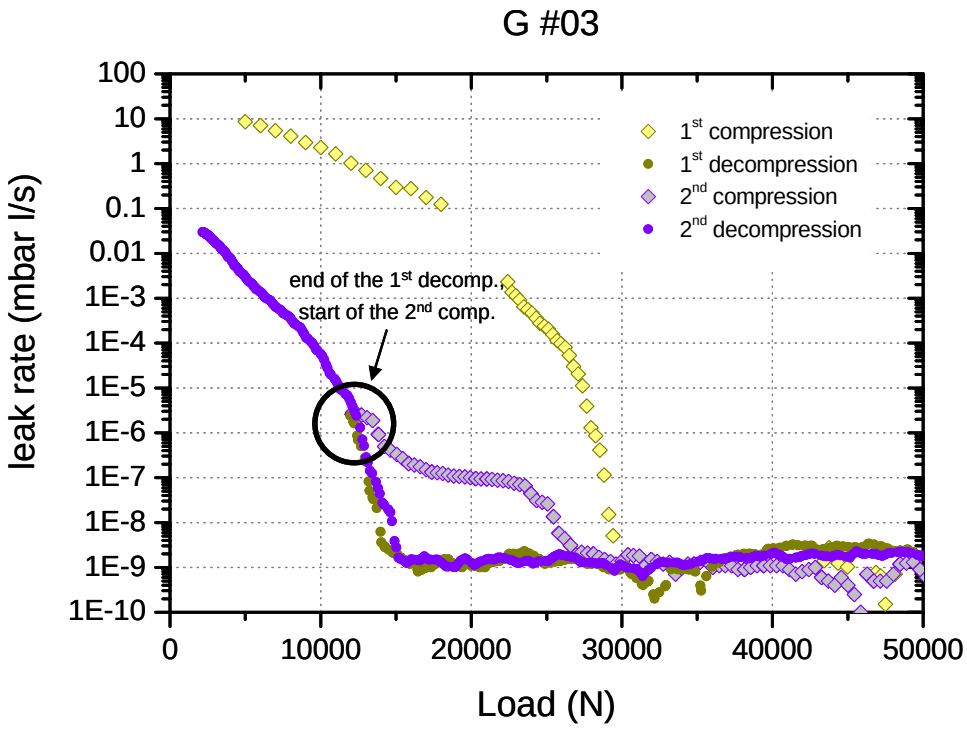

Figure 19: leak rate measurement during the compression and decompression test of gasket G #03 (Al6060).

This result has been obtained making the leak measurement during the entire test cycles, allowing the study of the sealing behavior not only for the first compression, but also in the following unloading and loading phases. It is evident that in the unloading phase the leak tightness is loosen at lower load level with respect to the one required for the generation of a leak tight seal during the first compression.

This type of measurement has been done on several gaskets. In Figure 20 the relation between the leak rate vs. load is shown. In particular it is evident the different behavior of the gaskets in Al6060 with respect to the Al5754 ones. The behavior of the leak rate at different loads measured with Al6060 and Al5754 gaskets give information on the compression force to be applied in order to ensure the seal tightening. The four steps in Figure 19 correspond to the following sealing stages: the accommodation of the seal, the normal sealing, and the reduction of the leak conductance by the increase of the local sealing [7]. With Al6060 the minimum load to apply for a leak rate $< 1 \cdot 10^{-9}$ mbarls^{-1} is 35 kN while using the Al5754 the minimum values is 42 kN. The reason of this is a consequence of the mechanical properties of the two different Al alloys. Al6060 has a lower flattening if compared with the Al5754. Therefore, at the same load, the pressure on the Al6060 gasket is higher than that for Al5754 one. Being the pressure on the gasket strictly related to the seal tightening, this would explain the necessity of higher load when using Al5754 gasket.

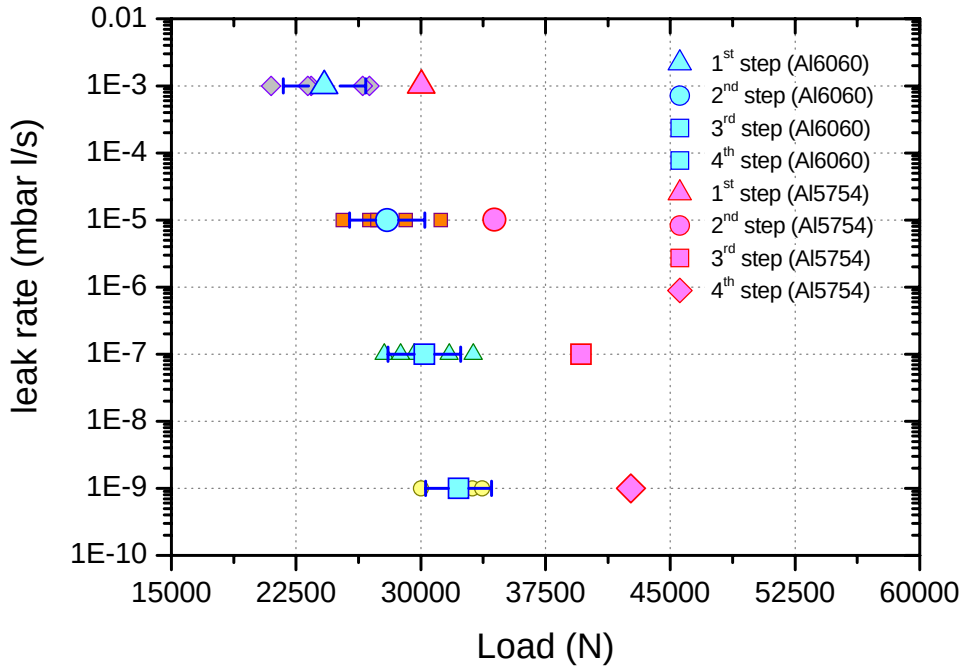

Figure 20: leak rate - compression load results after the removal of the background noise.

If the leak rate is plotted as a function of load together with the pressure as in Figure 21, it is evident that the seal is generated at about 35 kN, when the pressure on the contact area is of 550 MPa (about 91 N/mm).

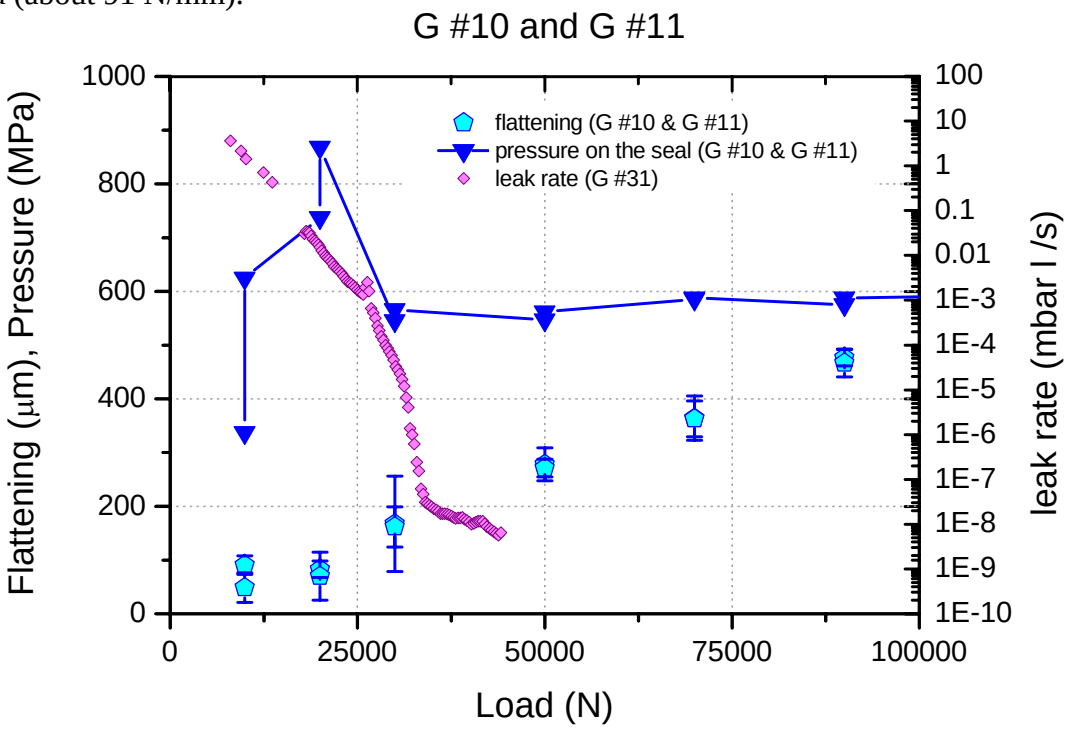

Figure 21: gasket flattening and pressure on G#10. The leak behavior refers to the same material type (G #31).

2.4 Compression test by manual tightening

Some tests by manual tightening have been performed at room and cryogenic temperature (liquid nitrogen). In the first case, the same stainless steel flanges used for the compression test with the Instron machine have been employed, while for the cryogenic tests the closed flange has been substitute with the NbTi one. CuNiSil nuts and stainless steel bolts and washers have been used, with the torque applied to the last.
A picture of the experimental set-up is shown in Figure 22. The aim of these manual measurements is to find an experimental relation between the results obtained with compression tests realized by the Instron machine with the one realized by manual tightening the TESLA beamline flanges.

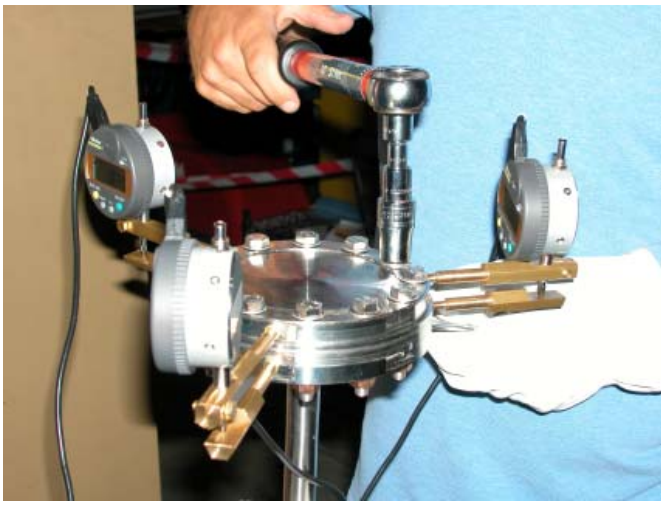

Figure 22 : manually compression test using a torque meter on the bolts head: the leak detector is connected to the bottom flange.

2.4.1 Test set-up

Like for the Instron compression measurements, we have tested gaskets belonging to the Al6060 and Al5754 families. Measurements of the elastic and plastic displacements have been obtained even using the electronic gauges and the manual micrometer (see Figure 23). All measurements have been done following the same experimental procedure, to avoid possible differences of friction or non-uniformity load during the gasket compression.
The standard procedure can be summarize in the following steps:

- gasket thickness measured before each compression test;
- bolts, nuts and washers cleaned, using the ultrasonic bath, with acetone for 10 minutes;
- new CuNiSil nuts for each measurement;
- damaged bolts never reused;
- torque tightening sequence well defined (see Figure 23);
- same gauges and micrometer position;
- permanent squashing of each gasket measured at the end of compression test with a micrometer in 4 points;
- flattening of each gasket measured in 4 points.

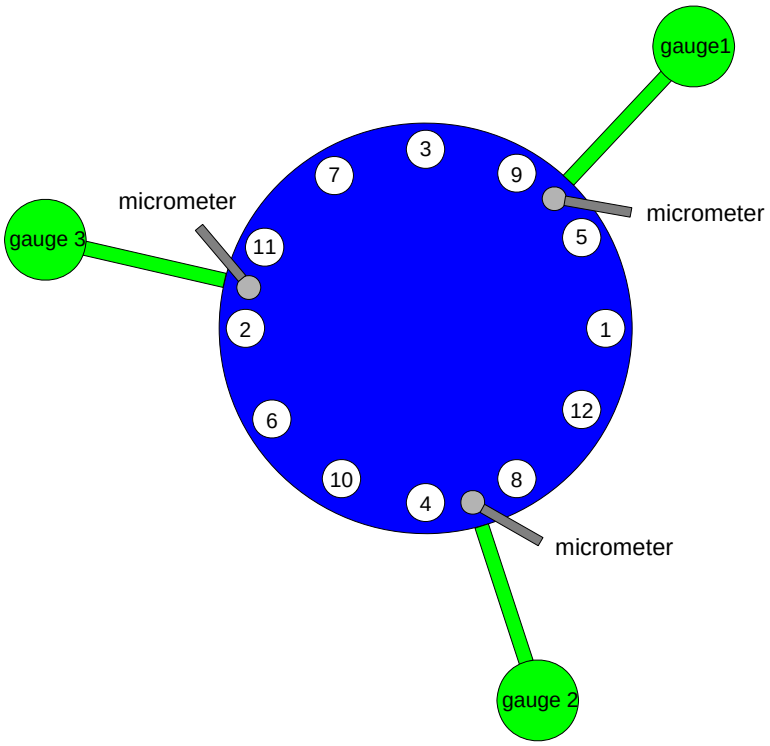

Figure 23 : sketch of the procedure followed during manual tightening. Numbers indicate the tightening sequence.

2.4.2 Torque – squashing results

Typical curves are shown in Figure 24, where two compression tests are reported. In the figure the mean displacements, measured both using the three gauges and the micrometer, are plotted for comparison. It is evident that gauges are affected by error due to the bending of the flanges.

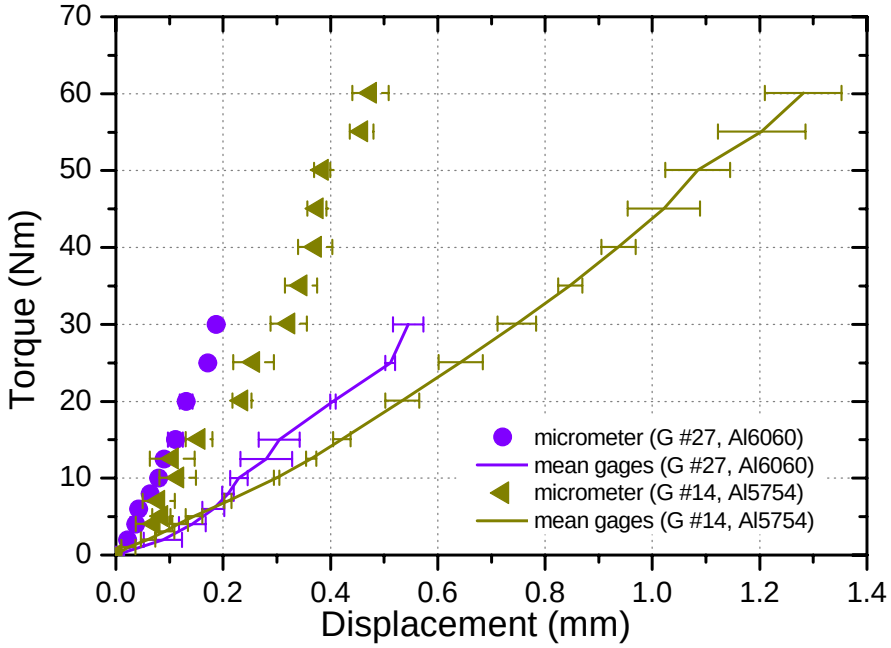

Figure 24: displacement vs. torque obtained for gasket G #14 (Al5754) and gasket G #27 (Al6060) by electronic gauges . Measurements done with the micrometer and the three gauges are compared.

2.4.2.1 Procedure followed to obtain the error curve

Following a procedure similar to the one used for the correction of the measurement done with the Instron machine (see section 2.3.2.1), we have calibrated our system using both the gauges and the micrometer. The obtained error curve is reported in Figure 25. In this case it is not necessary to use a non-linear initial fit for low torque value.

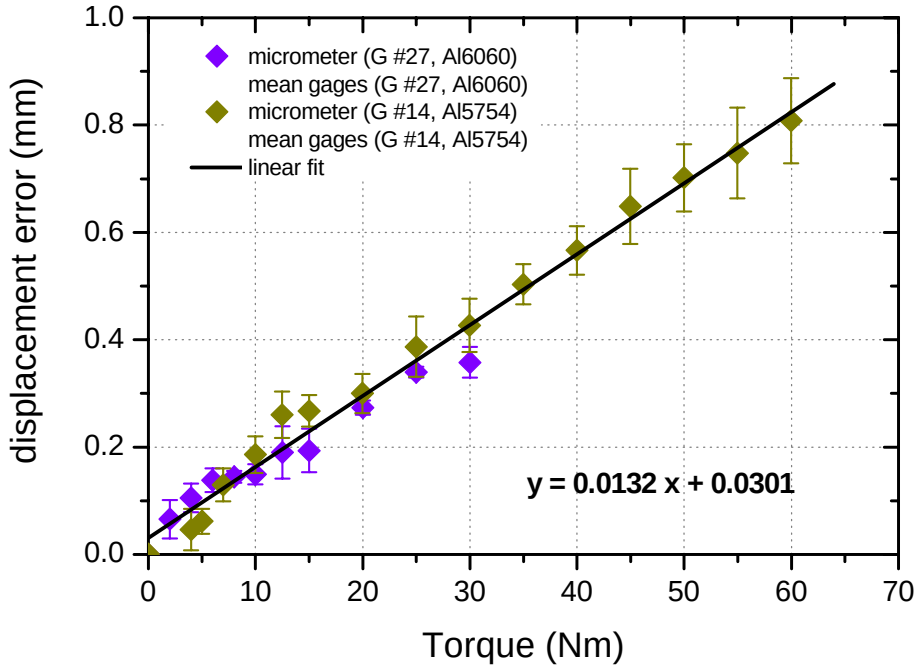

Figure 25: error curve of the displacement measured by gauges as a function of the torque applied.

2.4.2.2 Corrected compression measurement with bolts

The results of the manual tightening tests are here reported. In particular in Figure 26: and in Figure 27 results obtained with gasket G #27 (Al6060) and gasket G #38 (Al5754) are shown. In these plots we have reported not only the total displacement recorded at different torque, but also the permanent squashing and the elastic displacement of the gaskets. For these measurements the displacement has been obtained by the gauges during the unloading cycle at zero load.

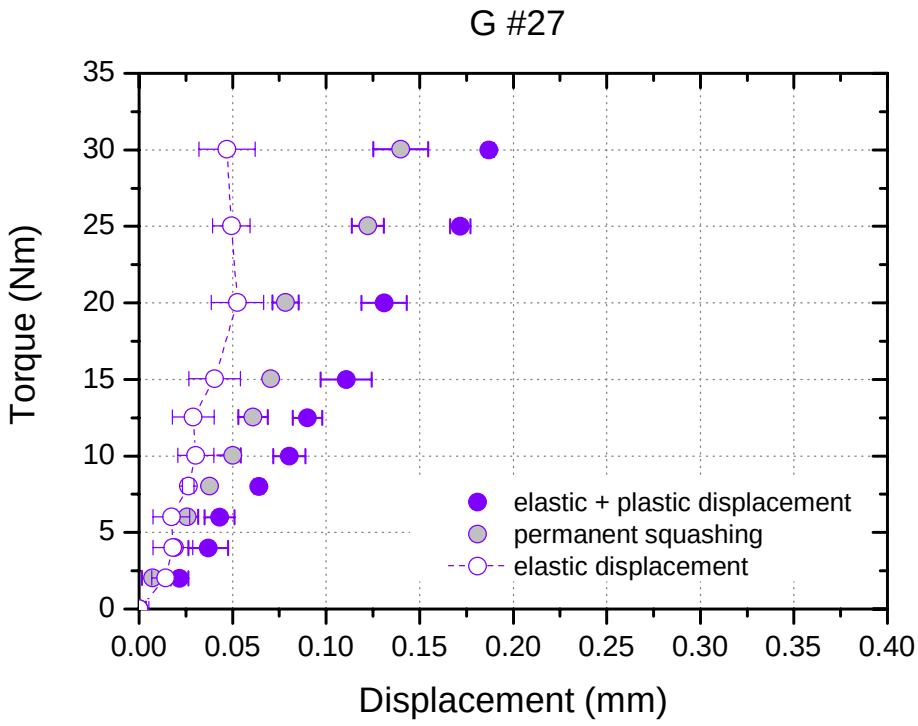

Figure 26: elastic and plastic displacement vs. torque of G #27 (Al6060).

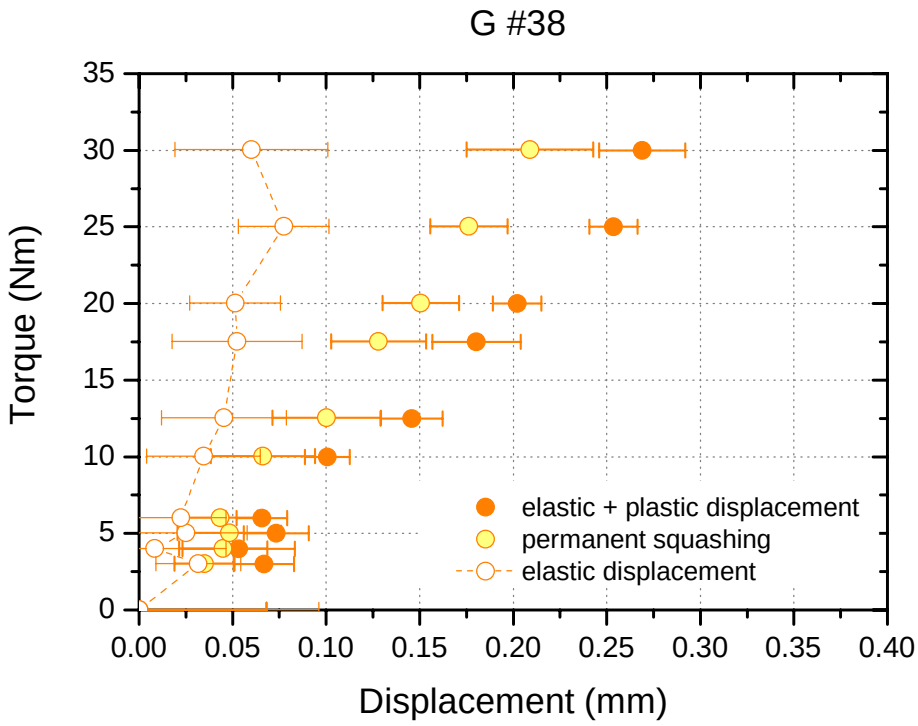

Figure 27: elastic and plastic displacement vs. torque of G #38 (Al5754).

The permanent squashing for all gaskets has been measured using the usual four points procedure and their values are reported in Figure 28.

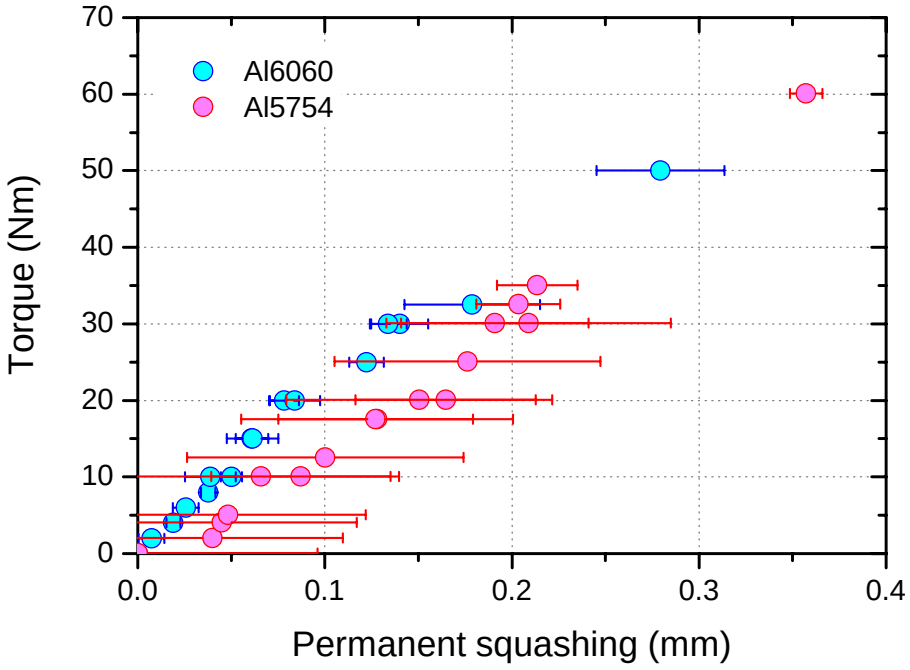

Figure 28 : permanent squashing of all gaskets tested by manual torque.

2.4.3 Flattening results

The flattening of the gaskets have also been measured after each test. The values are reported in Figure 29.

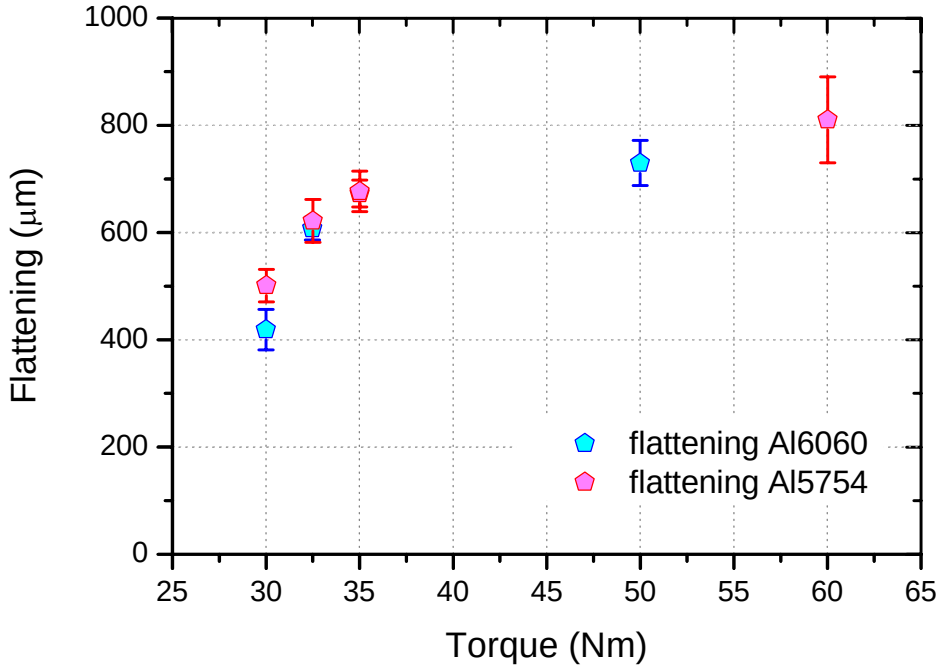

Figure 29 : flattening of several gaskets after the manual compression tests.

2.4.4 Leak rate result

Leak tests have also been performed during manual tightening. As an example, Figure 30 shows the leak rate behavior for the gasket G #40 (Al 5754 type) vs. torque. The connection is leak tight for a torque higher than 13 Nm.

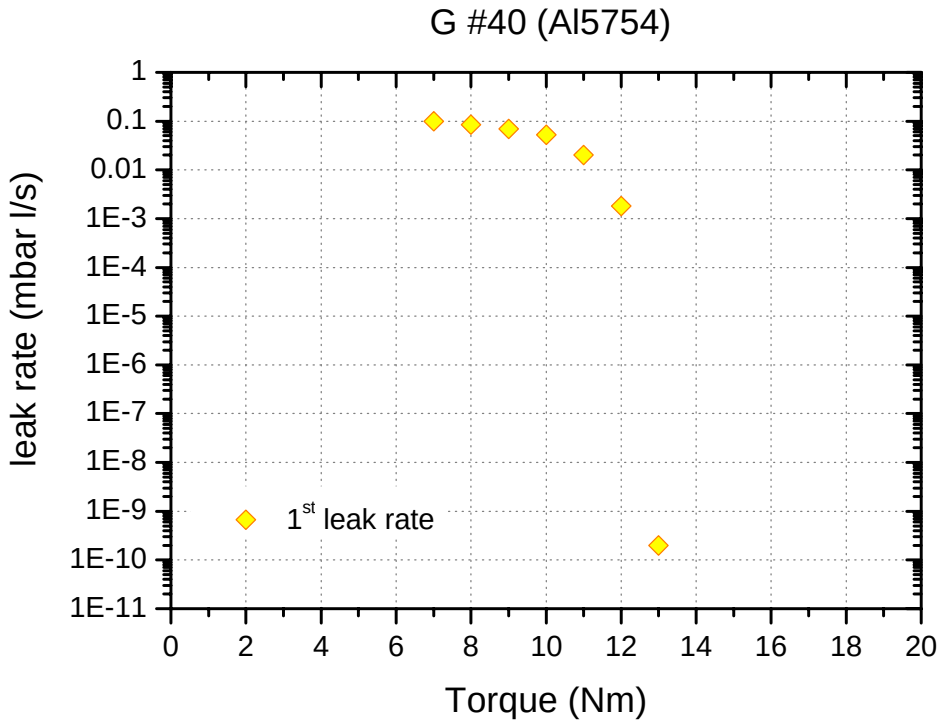

Figure 30 : leak rate vs. torque with G #40 - Al5754 gasket during the first compression.

2.5 Torque – compression force relation

A simple relation between force and torque can be obtained considering the load applied to a single bolts and the friction coefficient. Friction coefficient for common metals can be found on the literature: for our specific conditions (clean and degreased CuNiSil nuts and SS bolts) the friction is unknown and a different approach has to be used.

By comparing the measurement of the permanent squashing produced during the Instron tests with the one obtained from the flange manual tightening, we were able to obtain the torque-compression force relation and therefore the friction coefficient between the SS bolts and CuNiSil nuts in our particular conditions. The deformations measured with the Instron machine (Figure 15), and the one relative to the manual tightening (Figure 28) have been fitted with polynomial functions for an easier comparison (see Figure 31 and Figure 32).

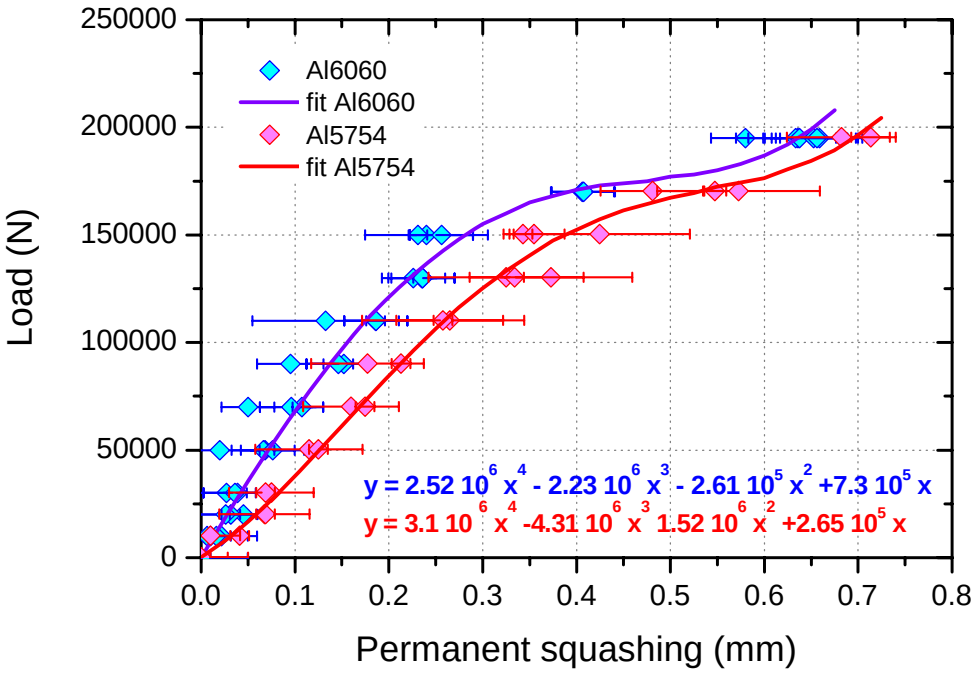

Figure 31 : permanent squashing as a function of the maximum force applied (Instron test).

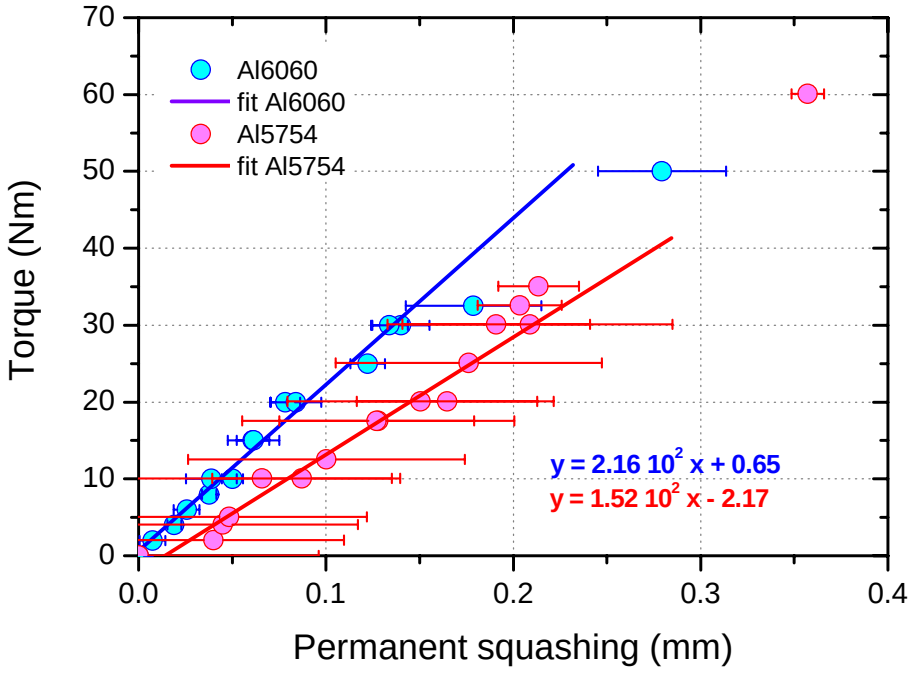

Figure 32 : permanent squashing as a function of the maximum load applied (manual tightening test).

The results of the manual tightening tests show a linear behavior up to 30-35 Nm. For higher value the behavior change and possible reasons could be the friction increase due to dust, nuts damage, etc.

The obtained relation between torque and force for our configuration (12 M8 bolts), has been plotted in Figure 33. Friction spans a range from 0.3 to 0.45, but for higher torque values friction increases up to 0.5.

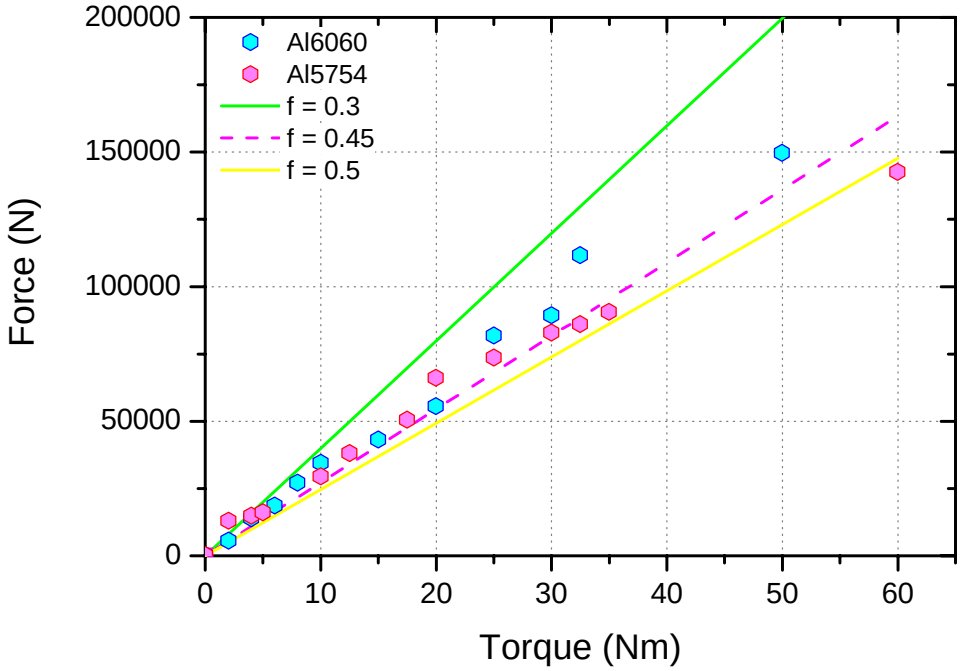

Figure 33: experimental relation between torque and compression force.

The relationship between torque and force obtained so far, lets compare in the usual force - displacement plane the information relative to the Instron compression tests with the ones obtained with the manual tightening (G #03 and G #37). This comparison is reported in Figure 34 and in Figure 35, respectively for an Al6060 (G #27) and an Al5754 (G #38) gasket.

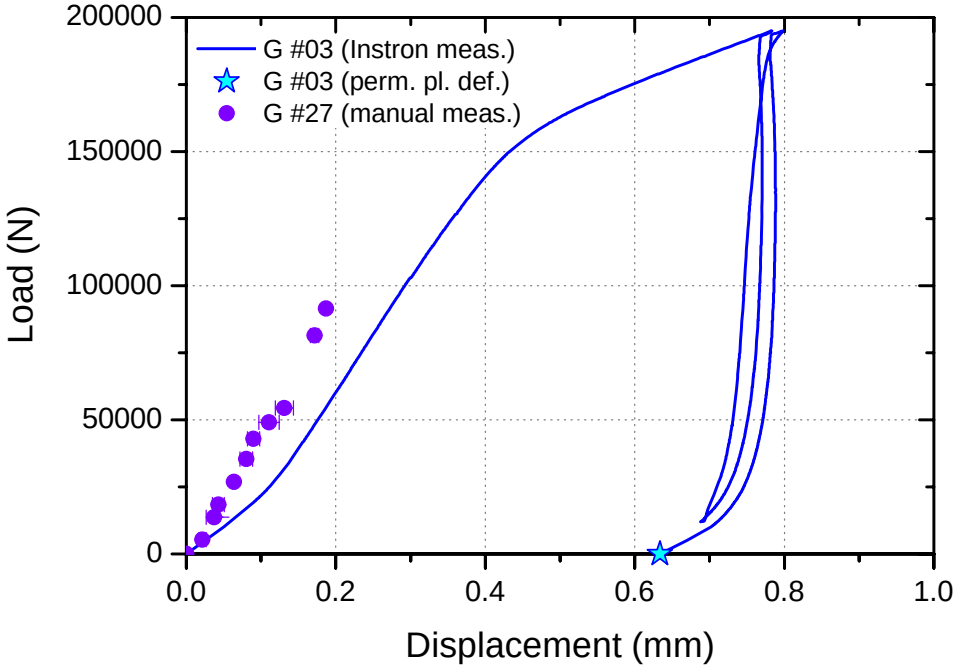

Figure 34 : Comparison between two compression tests for Al6060 gasket (G #27, hand tightening; G #03, Instron machine). The permanent squashing at zero load is also indicated.

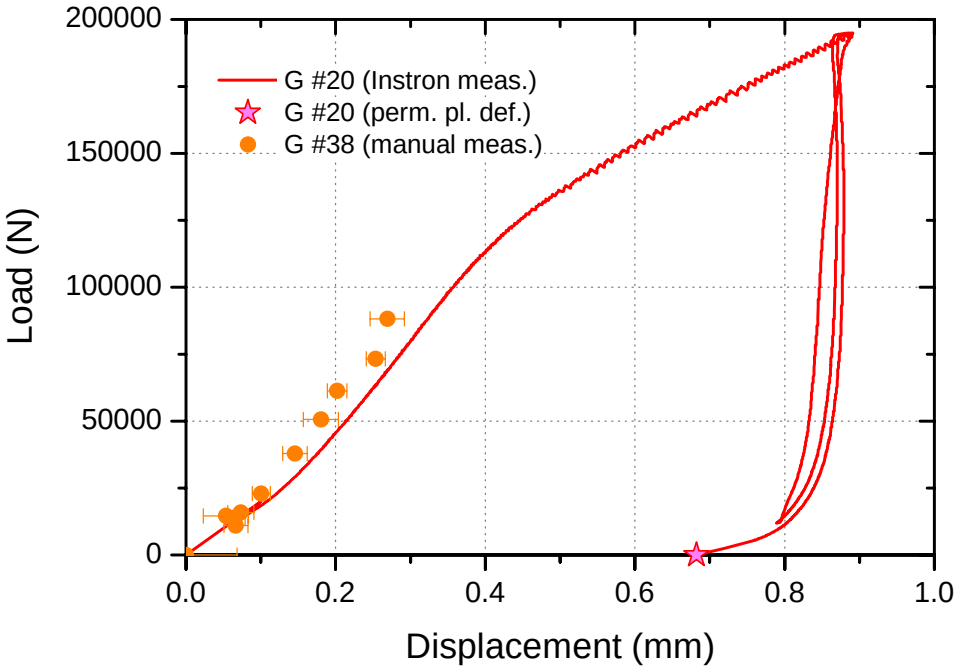

Figure 35: Comparison between two compression tests with Al 5754 gasket (G #38, hand tightening; G #20, Instron machine). The permanent squashing at zero load is also indicated.

2.5.1 An example

The typical torque value used during the TESLA beamline flange tightening (25 - 30 Nm [1]) corresponds to a total force applied to the flanges between 72 – 90 kN (see Figure 36).
Gasket squashing can be obtained referring to Figure 37. This correspond to a gasket shortening respectively of 0.10 – 0.14 mm for the Al6060 gaskets and 0.17 – 0.22 mm for the Al5754 ones. Moreover, the total displacement would be respectively 0.26 - 0.30 mm for the Al6060 gaskets and 0.28 - 0.33 mm for Al5754 ones.

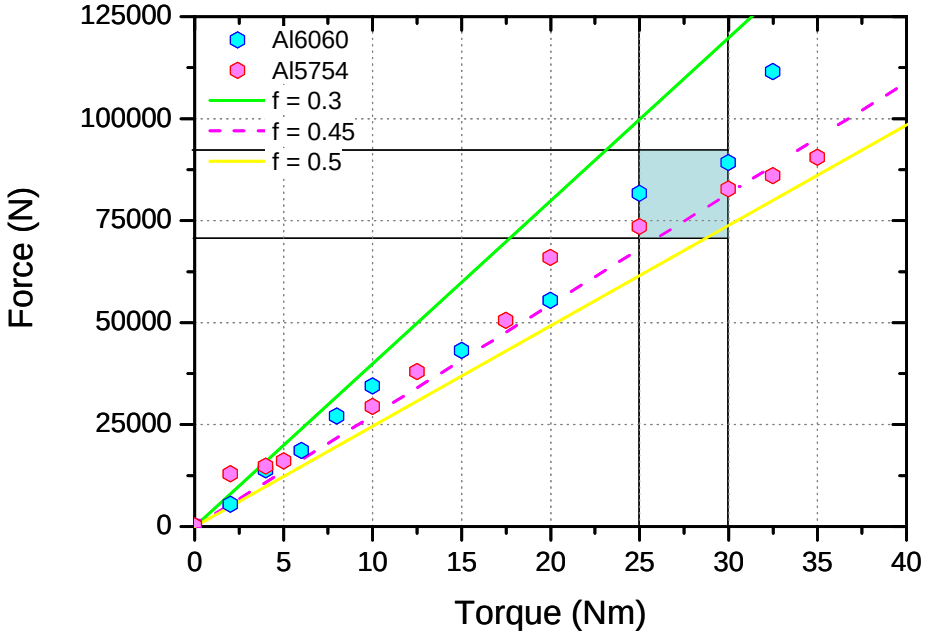

Figure 36: conversion torque - force. The TESLA flange tightening range (between 25 and 30 Nm) is indicated in the white blue rectangle. In the plot also the corresponding friction is reported.

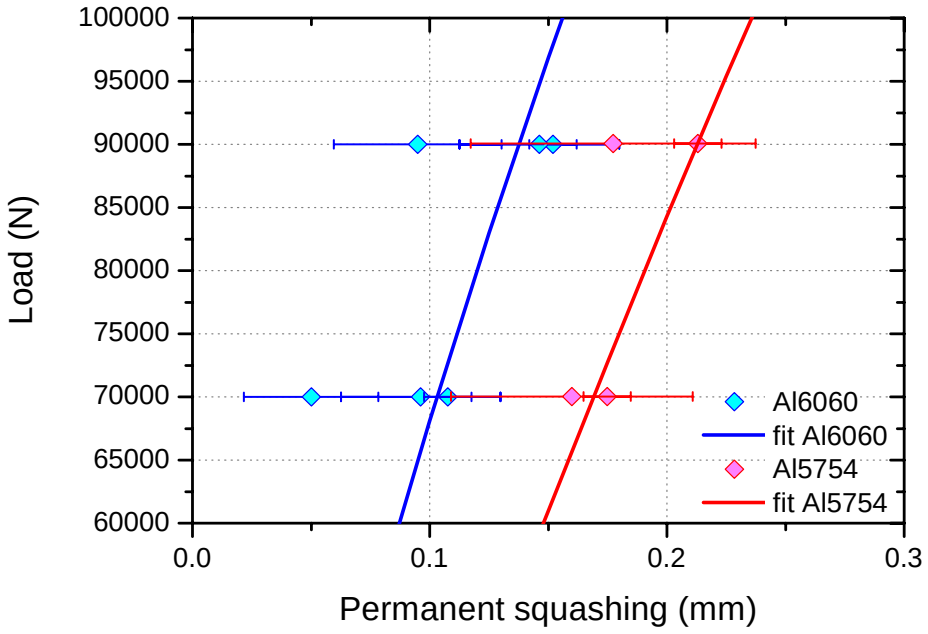

Figure 37: permanent squashing vs. force.

2.6 Cryogenic leak tests

Compression tests at cryogenic temperature (77K), not possible with the Instron material testing machine, have been performed using a suitable experimental set-up (see Figure 38). We used two different materials (SS and NbTi) for the flanges in order to simulate the TESLA beamline flanges behavior.

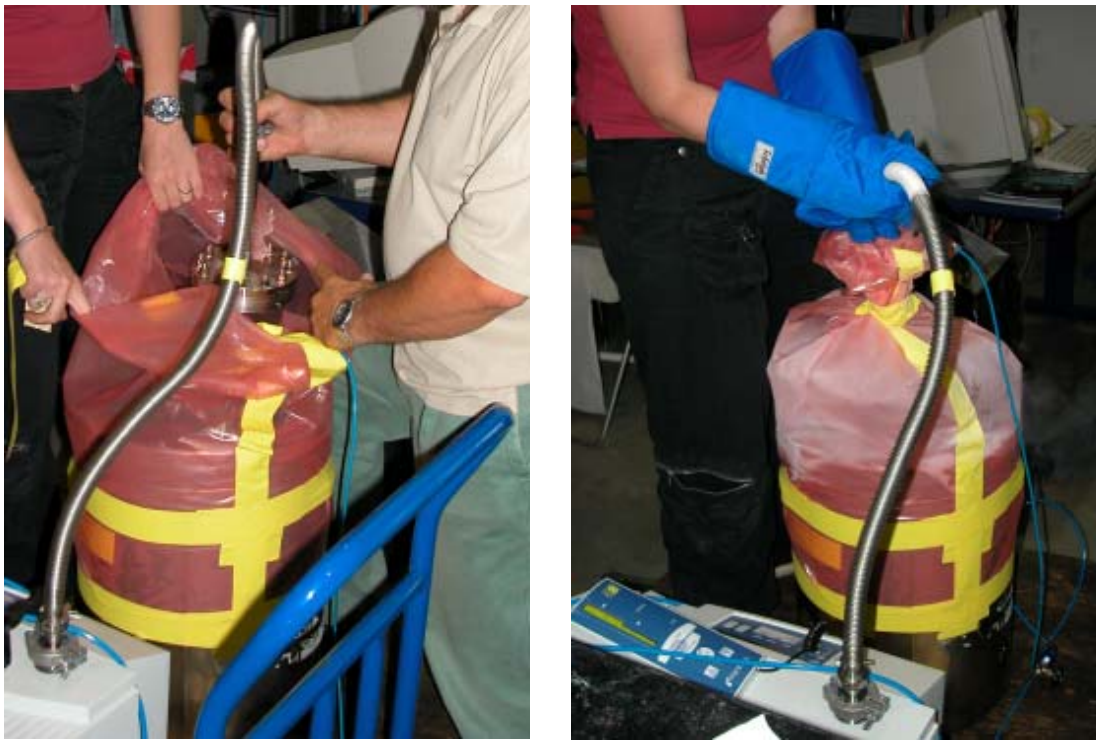

Figure 38: picture of the experimental set-up for cryogenic measurements.

The flanges have been tightened applying the minimum torque needed to generate a leak tight joint (leak rate less than $1 \cdot 10^{-9}$ mbarls^{-1}), checking the presence of leaks during thermal cycles. The joint was immersed in liquid nitrogen, and let cooling down. The connection system was removed from the LN_2 bath and immediately leak checked. A plastic bag was used both for the confinement of the helium during the test and to avoid any water vapor condensation that may affect the quality of the measurement. This procedure has been repeated several times on the same flanges-gasket system to study the tightening seal behavior after several thermal cycles. Between one thermal cycle and the other we let warming up the joint up to room temperature.

At the present, we have tested only few gaskets and the results obtained have to be considered as preliminary. In one case (G #40, Al5754 gasket type), the torque necessary to have a leak tight seal was 13 Nm. At cryogenic temperature, the system presented a leak of $2 \cdot 10^{-5}$ mbarls^{-1} that disappeared when the system got back to room temperature. With G #04 (Al6060), the torque necessary to have leak tightness was 10 Nm. In this case we did not measured any leak during two temperature cycles.

After the thermal cycles the gaskets squashing were checked: both presented an increase in squashing respect to the one foreseen at room temperature for the applied torque, indicating an increase of the load applied to the flanges during the cooldown.

3 Finite element simulations

A finite element model has been developed in order to foresee the connection behavior. This model has then been validated by comparison with the experimental tests presented in section 2.

3.1 Material characteristics

The mechanical characteristics of flanges and gasket used for the numerical simulation have been collected in Table 2. A graphical explanation of symbols used is reported in Figure 39.

Materiale	E_y (MPa)	ν	f_y (MPa)	ε_y	E_t (MPa)	f_t	ε_t
AISI 304/316	191000	0.29	342	0.179%	939	716	40.0%
NbTi	62055	0.25	483	0.778%	301	552	23.7%
AlMg3	69000	0.26	110	0.159%	352	201	26.0%
AlMgSi05	70000	0.26	196	0.229%	312[†]	246	17.0%

Table 2: room temperature mechanical characteristics used in numerical simulations.

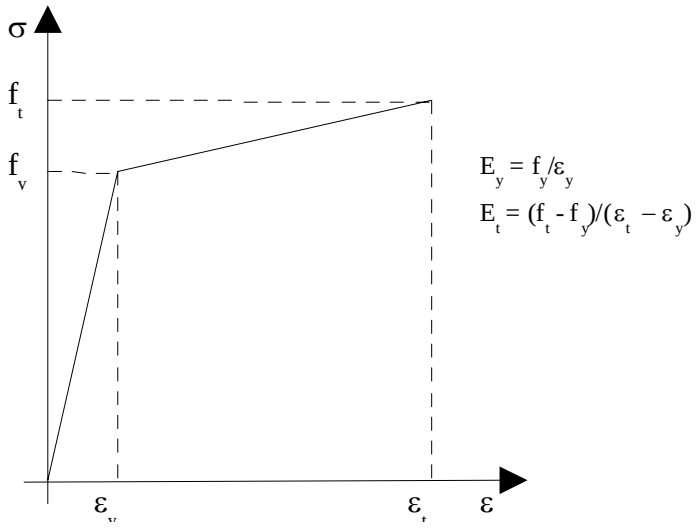

Figure 39: bilinear elasto-plastic behavior used in numerical simulations.

3.2 Finite element model

The simulations have been performed by means of the commercial code Ansys®. The following settings have been used:

- static analysis with axisymmetric model
- geometric nonlinearity and stress-stiffening considered;
- elasto-plastic material (bi-linear with Rice's hardening rule);

The model of the connection consists of 1787 PLANE82 elements, 82 TARGE169 elements, 237 CONTA175 elements and a total of 5822 nodes (see Figure 40). The particulars of the boundary conditions and contact element are reported in Figure 41 and Figure 42.

[†] Values taken from the material certificate

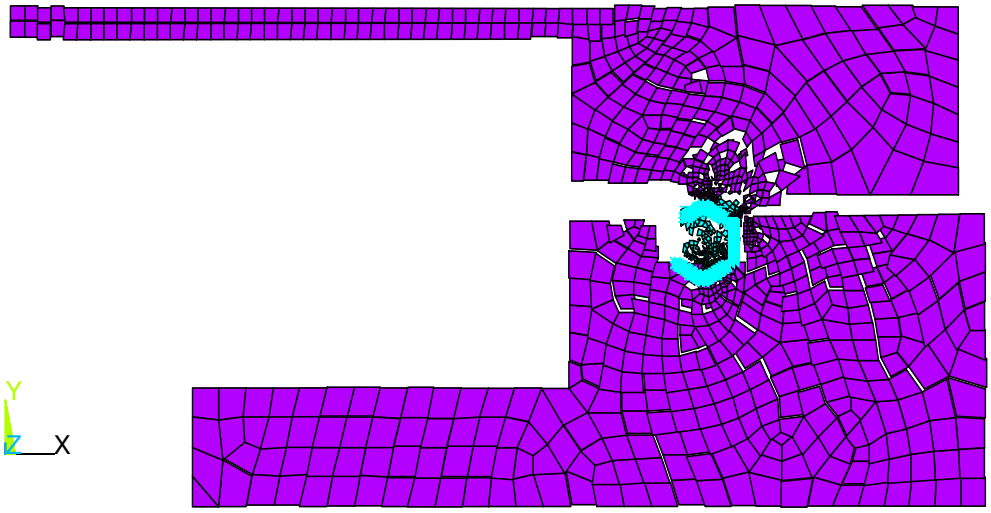

Figure 40: finite element model of the beamline connection.

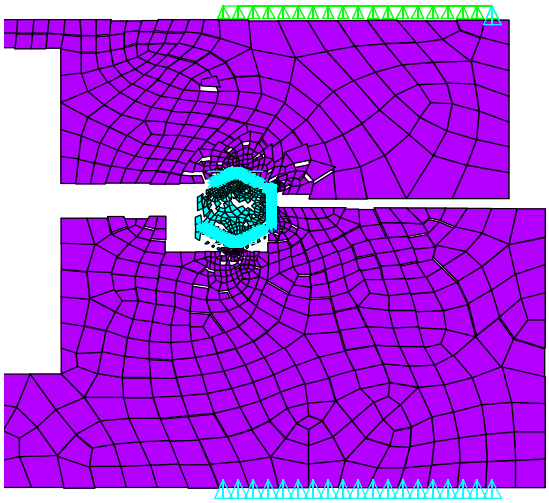

Figure 41: particular of boundary conditions.

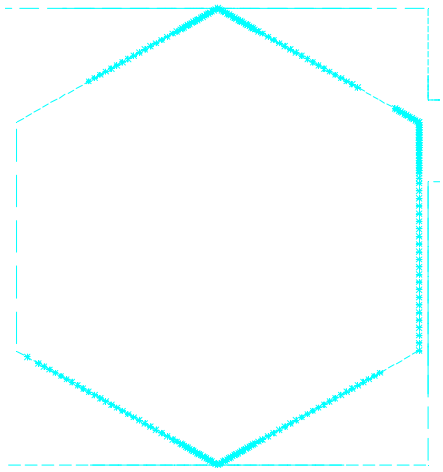

Figure 42: particular of contact elements.

3.3 Results

A finite element analysis has been performed for the gasket in AlMgSi0.5 (or Al5754) because experimental mechanics characteristics are available. The force – squashing curve is reported in Figure 43 where the distribution of the equivalent plastic strains is also plotted at three different levels. The connection closure by means of 12 bolts make the gasket squashing : plastic strains develop soon due to the almost linear contact between the gasket and the groove.

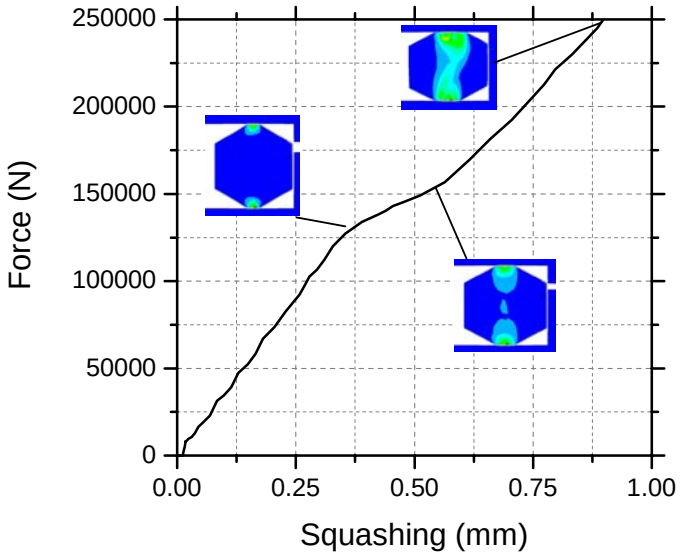

Figure 43: results of finite element analysis.

As the compression force grow, the flattening increase and the mean pressure on the gasket is varying as highlighted in Figure 44.

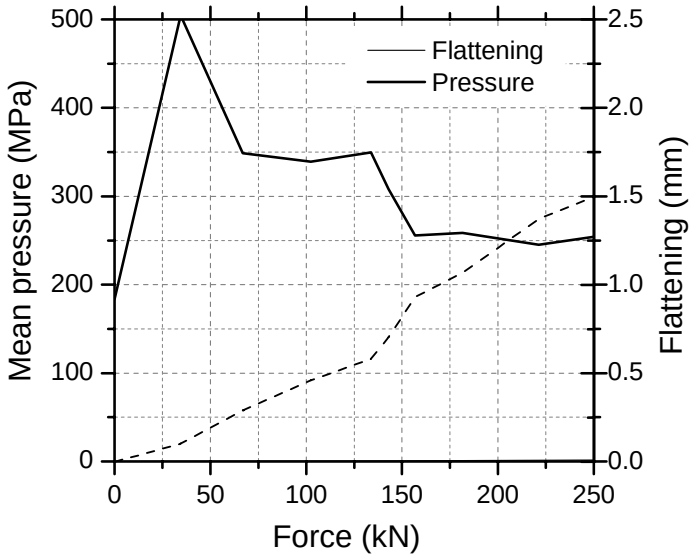

Figure 44: flattening and pressure of gasket sealing surface during compression.

The von Mises stress and the equivalent plastic strain in the gasket for a compression force of 80 kN (approximately 28 Nm of torque on any bolt) are reported in Figure 45 and Figure 46.

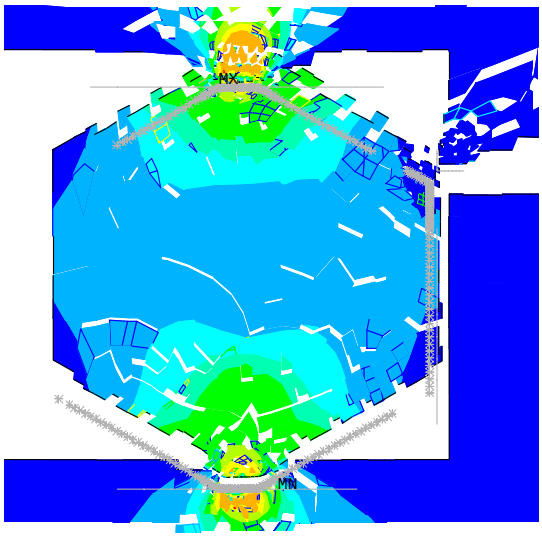

Figure 45: von Mises stress (80kN).

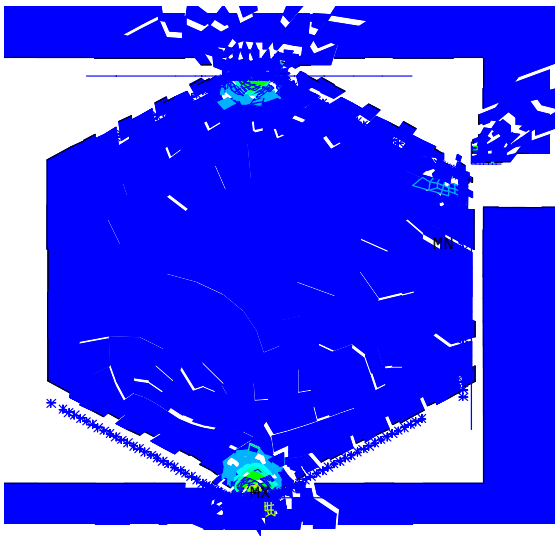

Figure 46: equivalent plastic strain (80kN).

4 Influence of temperature: a simple analytical model

4.1 Hypotheses

In this section an analytical model of flanged connections allowing to consider temperature effects is presented. In particular the TTF beamline connection simplified geometry is taken as reference (see Figure 47).

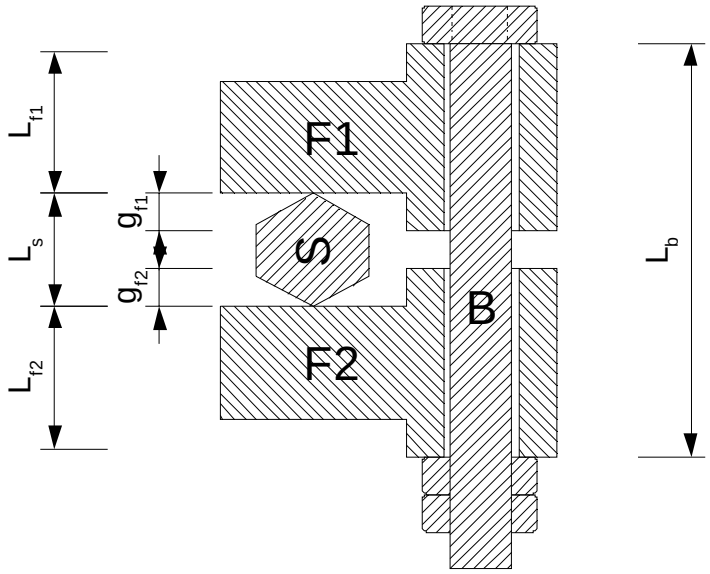

Figure 47: TTF beamline connection scheme.

The model is obtained by imposing equilibrium and congruence to the connection when the following hypotheses are true:

- the bending variation of flanges are negligible;
- the elastic deformations of flanges are negligible;
- the bolt behave in linear elastic way (Hooke's elastic law)

4.2 The model

Now, let us consider the connection closed by a force F_0 (compression is negative) on the seal due to the traction N_{b0} on the n_b bolts such that the seal height and the bolt length will be equal to L_{s0} and L_{b0} (see Figure 48):

$$N_{b0} = -\frac{F_0}{n_b} \tag{1}$$

In writing this relation tensile forces are considered positive. In the same way the deformations will be considered positive when the material is subjected to an elongation.
If a thermal variation is applied, the connection will move in a different configuration characterized by a variation of force ΔF and elongation Δe. For congruence the following equation can be written, where the variation symbol Δ has been omitted for simplicity:

$$e_b = e_s + e_{f1} + e_{f2} \tag{2}$$

where *b*, *s* and *f* refer respectively to bolts, seal and flanges and any elongation is composed of three parts, the thermal, the elastic and the plastic ones:

$$e = e_t + e_e + e_p \tag{3}$$

Therefore:

- the bolts have not plasticity: $e_b = e_{bt} + e_{be}$
- the flanges have only thermal deformations: $e_f = e_{ft}$

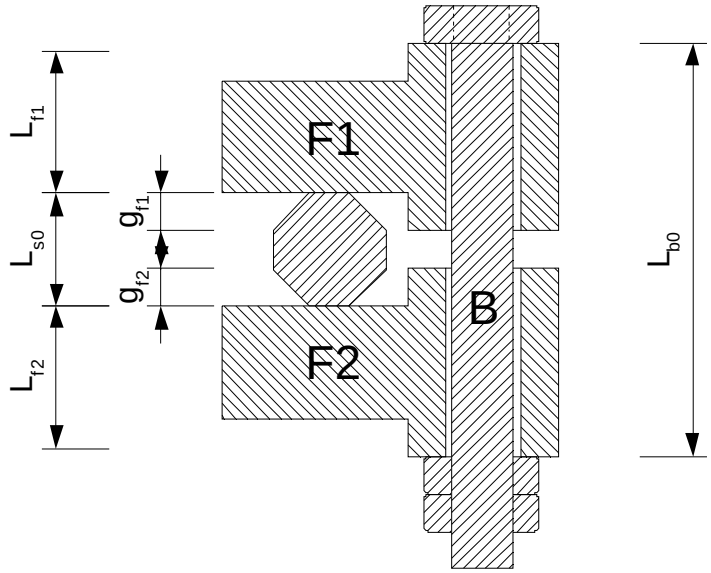

Figure 48: TTF beamline connection scheme in compressed configuration.

Expanding equation (2) and grouping the terms we obtain the relation (4), where the left hand term represents the variation of space at available for the seal due to the temperature variation, while the right hand term represent the strains variations due to the new equilibrated and congruent configuration:

$$e_{bt} - e_{f1t} - e_{f2t} - e_{st} = e_{se} + e_{sp} - e_{be} \tag{4}$$

Obviously relation (5) must be satisfied for equilibrium:

$$\Delta N_b = -\frac{\Delta F}{n_b} \tag{5}$$

If material characteristics and their thermal deformation are known, therefore the elongation can be expressed in terms of ΔT and ΔF:

$$\begin{aligned} e_{bt} &= \Delta_{bt} L_{b0} & e_{be} &= (\Delta N_b L_{b0})/(E_b A_b) \\ e_{f1t} &= \Delta_{f1t} L_{f1} & e_{se} &= e_{se}(\Delta F; F_0) \\ e_{f2t} &= \Delta_{f2t} L_{f2} & e_{sp} &= e_{sp}(\Delta F; F_0) \\ e_{st} &= \Delta_{st} L_{s0} \end{aligned} \tag{6}$$

where Δ_t are the thermal deformation for a known temperature difference and $e_s(\Delta F;F_0)$ are obtained by experimental test or finite element analyses.
Applying the relations (6), the equation (4) becames:

$$e_t(F_0;\Delta T) = e_s(F_0;\Delta F) - e_b(F_0;\Delta F) \tag{7}$$

and if the equilibrium condition (5) is used, it is possible to obtain the final relations between the temperature variation and the new configuration of the connection:

$$e_t(F_0;\Delta T) = e_s(F_0;\Delta F) + \frac{\Delta F \cdot L_{b0}}{n_b E_b A_b} \tag{8}$$

Depending on the form of e_s, the equation (8) can be solved explicitly or by means of iterative algorithms.

4.3 An example

Let us consider the TTF beamline connection and the seal deformations obtained by means of experimental test explained in section 2.
We consider an initial closure torque of 30 Nm applied to the 12 bolts.

Δ_{f1t} = -1.9 E-3 (NbTi) from room temperature to LHe

Δ_{f2t} = -3.0 E-3 (AISI304) from room temperature to LHe

Δ_{st} = -4.15 E-3 (AlMg3) from room temperature to LHe

Δ_{bt} = -3.0 E-3 (AISI316) from room temperature to LHe

L_{f1} = 11.5 mm

L_{f2} = 16.5 mm

L_{s0} = 5.00-0.32 = 4.68 mm (from Figure 24)

L_{b0} = 28.0 mm + L_{s0} = 32.68 mm

F_0 = 93180 N (from figure Figure 33)

In the cool down to the liquid helium temperature the thermal elongation are:

e_{bt} = -3.0 E-3 *32.68 = -0.09804 mm

e_{f1t} = -1.9 E-3 *11.5 = -0.02185 mm

e_{f2t} = -3.0 E-3 *16.5 = -0.04950 mm

e_{st} = -4.15 E-3 *4.68 = -0.01942 mm

for a total $e_t(F_0;\Delta T)$ = -0.00727 mm.

From Figure 13, opportunely reported here (Figure 49), it can be seen that for sufficiently small variation ΔF from F_0 the variation in length is $e_s(F_0;\Delta F)$ = (0.36-0.22)/50000 ΔF, where e_s and ΔF are measured in mm and N. Using equation (8) the variation ΔF can be obtained:

$$-0.00727 = \left(\frac{0.36-0.22}{50000} + \frac{32.68}{12 \cdot 191000 \cdot 36.1} \right) \Delta F \Rightarrow \Delta F = -2275N$$

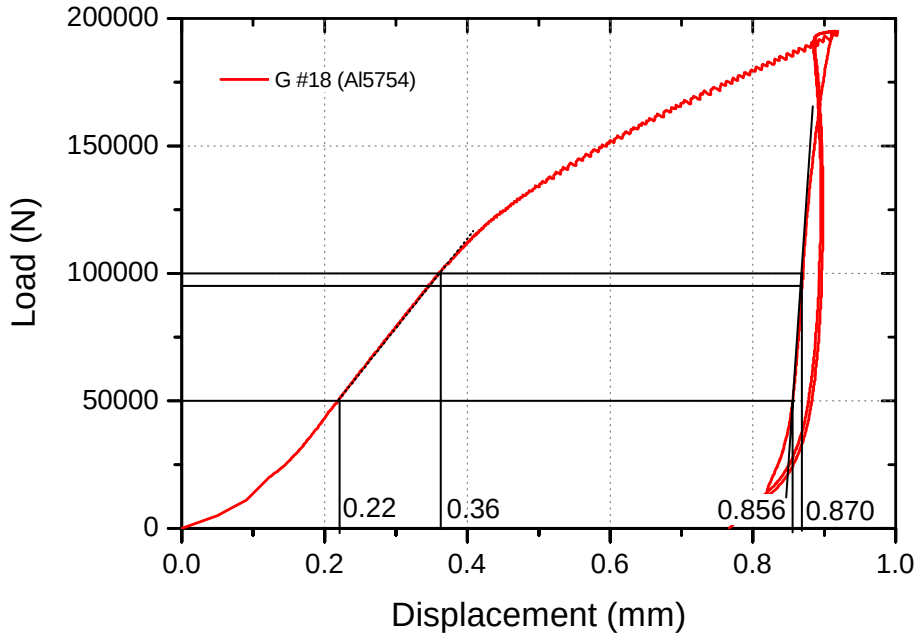

Figure 49: approximation of gasket elongation.

The value obtained is sufficiently small, as required from the hypothesis previously described, and the negative value means that the gasket is more compressed than at room temperature. Now the elongation of gasket and bolts can be easily obtained:

$$e_s(F_0;\Delta F) = \frac{0.15}{50000}(-2275) = -0.00682\ \text{mm}$$

$$e_b = \frac{2275 \cdot 32.68}{12 \cdot 191000 \cdot 36.1} = 0.00090\ \text{mm}$$

This example shows how the variation of temperature has a negligible influence on the closure of the connection.

Let us suppose now to warm up from LHe to room temperature: the just evaluated plastic part of the additional deformation e_s has to be recovered by the elastic behavior of the gasket which unloads during this phase. In order to evaluate the final conditions, it is possible to apply the relation (8) paying attention to change the expression of $e_s(F_0;\Delta F)$ because the gasket is going to follow the unloading path. Therefore:

$$e_s(F_0;\Delta F) = (0.870 - 0.856)/50000\ \Delta F$$

$$+0.00727 = \left(\frac{0.87 - 0.856}{50000} + \frac{32.68}{12 \cdot 191000 \cdot 36.1}\right)\Delta F \Rightarrow \Delta F = 10771N$$

and the gasket unload by 10771 N, going to a final compression load of 95455 – 10770 = 84685 N.

This value is higher than the minimum required for the sealing. If other thermal cycles are applied to the connection, the gasket compression will vary between 84685 N and 95455 N without develop other plastic strains.

5 Conclusion and future development

An in deep study of the behavior of the Tesla beamline connection has been performed. We have obtained the permanent squashing, the elastic recovery, the behavior of the leak rate versus the force and the friction coefficient between the SS bolt and the CuNiSil nut.
Furthermore the test results allowed to validate a finite element model of the connection (see Figure 50). This can be used for future study and optimization of new seal geometry and material.

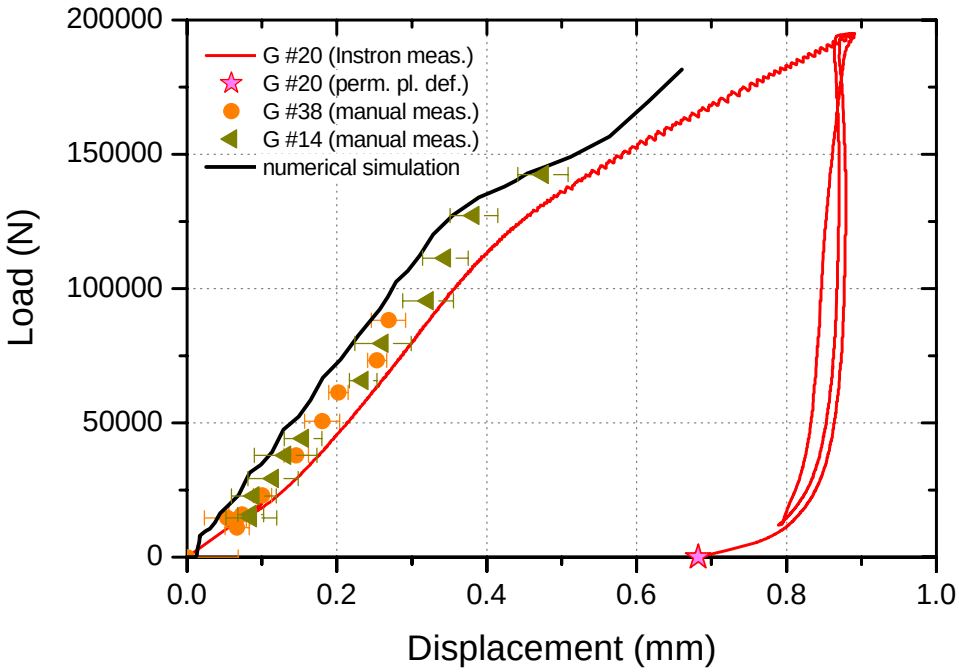

Figure 50: comparison between the numerical model results and the experimental data.

Using the model presented in section 4, the temperature effects can be taken into account and some useful indications for the future development can be drawn. In particular, temperature cycling load (cool down and warm-up) can induce, and this is the case for the beamline connection, additional deformations to the gasket and the plastic part will not be recovered. The value of this deformation has to be sufficiently small in order to prevent leaks when the temperature, after a cool down, return to the room value. A good design of the connection geometry (overall thickness of flanges and gasket) could lead to a null additional deformations and in this case the temperature variation does not will affect the seal of the gasket.
The actual geometry seems to be well designed. As a matter of fact, a typical temperature cycle produces a compression force variation of 10 kN, that can be compensated by the elasticity of the gasket used. An improvement on the flanges performances can be obtained with new optimized geometry (flanges thickness, seal shape) or using different materials able to better compensate the temperature effects.
Finally, the results obtained and presented in this report could be used as a reference point for the design of a new fast clamping device that nowadays is still one of the unresolved problem for the future superconducting linear accelerators.

6 Acknowledgements

We acknowledge M. Todero for the support given during the experimental tests with the material testing machine.
We acknowledge the support of the European Community-Research Infrastructure Activity under the FP6 “Structuring the European Research Area” programme (CARE, contract number RII3-CT-2003-506395).

7 Reference

[1] P. Michelato, L. Monaco, R. Paulon, “Improved Standard Cavity Fabrication”, CARE Note-05-003-SRF, 2005.
[2] T. M. Rothgeb, P. E., R. B. Overton, “Cycling Testing of The SNS DESY Style Seals”, JLAB-TN-02-052.
[3] J.-C. Brunet, A. Poncet, P. Trilhe, “Leak-tightness assessment of demountable joints for the super fluid helium system of the CERN Large Hadron Collider (LHC)”, Adv. in Cryog. Eng., Vol. 39, Plenum Press, 1994.
[4] H. Tatsumoto, K. Saito, H. Inoue, Y. Kobayashi, “Simple aluminium sealing against superfluid helium”, Proc. SRF 2003, Lubeck.
[5] K. Zapfe-Duren, F. Hermann, D. Hubert, P. Schmuser, ”A new flange design for the superconducting cavities for TESLA“, Proc. 8th workshop on RF superconductivity, Abano Terme, 1997.
[6] A. Roth, “Vacuum sealing techniques”, AIP Press, 1994.
[7] A. Roth, “Vacuum technology”, second revised edition, North-Holland, 1982.